Electronic Supplementary Material (ESI) for ChemComm.

Electronic Supporting Information

Are the Orientation and Bond Strength of the RCO_2^- • • • M Link Key Factors for Ultrafast Electron Injection in DSSCs?

Peng Luo, Paul-Ludovic Karsenti, Gessie Brisard, Benoît Marsan and Pierre D. Harvey

Table of content

Experimental Section

Materials

The $[Pd_3(dppm)_3(CO)](PF_6)_2$ cluster, **$[Pd_3^{2+}]$**,[1a] 5-(4-carboxylphenyl)-10, 15, 20-tritolyl-(porphyrinato)zinc(II)[1b] and 5, 15-(4-carboxylphenyl)-15, 20-(tolylporphyrinato)zinc(II)[1c] were prepared according to literature procedures. Carboxylate sodium salts **MCP** and **DCP** were synthesized by ion-exchange resin from their acid counterparts.[2]

Electrochemical Measurements

Electrochemical measurements were conducted with a three-electrode potentiostat (Princeton, Applied Research Corporation, Model 273A) in solvents deoxygenated by purging with purified Ar gas. Cyclic voltammetry was obtained by using a three-electrode cell equipped with a glassy carbon disk (0.07 cm^2) as the working electrode, a platinum wire as auxiliary electrode, and a Ag/Ag^+ electrode as reference electrode at 298 K. The working electrode was polished with aluminium (0.03 μm) on felt pads (Buehler) and treated ultrasonically for 1 min before each experiment. The reference electrode was separated from the bulk solution with a double junction filled with electrolyte solution. The reproducibility of individual potential values was within ± 5 mV. Tetra-*n*-butylammonium hexafluorophosphate ($TBAPF_6$) was used as supporting electrolyte, which was obtained from Sigma-Aldrich, and used without further purification. Ferrocene/ferrocenium (Fc/Fc^+) was used as internal standard. Potentials measured *vs* Ag/Ag^+ electrode were converted to those for saturated calomel electrode (SCE) for comparison.

Calculation Procedure

All density functional theory (DFT) and time dependent density functional theory (TD-DFT) calculations were performed with Gaussian 09[3] at the Université de Sherbrooke with the Mammouth supercomputer supported by *Le Réseau Québécois De Calculs Hautes Performances*. The DFT geometry optimizations as well as TD-DFT calculations[4-13] were carried out using the B3LYP method. A 6-31g* basis set was applied to C, H, N, O, Na atoms in porphyrins alone, while a 3-21g* basis set was used for C, H, N, O, P atoms in palladium cluster and its assembly with porphyrins. VDZ (valence double ζ) with SBKJC effective core potentials were used for all Zn and Pd atoms .[14-19] All calculations were carried out in a methanol solvent field. The calculated absorption spectra were obtained from GaussSum 2.1.[20]

Instruments

Absorption spectra were measured on a Varian Cary 300 Bio UV-Vis spectrometer at 298K and on a Hewlett-Packard 8452A diode array spectrometer with a 0.1 second integration time at 77K. Steady state fluorescence and excitation spectra were acquired on an Edinburgh Instruments FLS980 phosphorimeter equipped with single monochromators. All fluorescence spectra were corrected for instrument response. Fluorescence lifetime measurements were made with the FLS980 phosphorimeter using a 378 nm picosecond pulsed diode laser (fwhm = 90 ps) as an excitation source. Phosporescence lifetime measurements were aquired on the FLS980 using a microsecond flashlamp set with a 515 nm excitation. Data collection on the FLS980 system is done by time correlated single photon counting (TCSPC).

Femtosecond transient absorption spectroscopy

The fs transient spectra and decay profiles were acquired on a homemade system using the SHG of a Soltice (Spectra Physics) Ti-sapphire laser (λ_{exc} = 398 nm; fwhm = 75 ps; pulse energy = 0.1 μJ per pulse, rep. rate = 1 kHz; spot size ~ 500 μm), a white light continuum generated inside a sapphire window and a custom made dual CCD camera of 64 × 1024 pixels sensitive between 200 and 1100 nm (S7030, Spectronic Devices). The delay line permitted to probe up to 4 ns with an accuracy of ~4 fs. The results were analysed with the program Glotaran (http://glotaran.org) permitting to extract a sum of independent exponentials ($I(\lambda,t) = C_1(\lambda) \times e^{-\frac{t_1}{\tau}} + C_2(\lambda) \times e^{-\frac{t_2}{\tau}} + \cdots$) that fits the whole 3D transient map.

References

(1) (a) L. Manojlovic-Muir, K. W. Muir, B. R. Lloyd, and R. J. Puddephatt. *J. Chem. Soc., Chem. Commun.*, 1983, **22**, 1336. (b) A. S. Hart, C. B. KC, H. B. Gobeze, L. R. Sequeira, and F. D'Souza. *ACS Appl. Mater. Interfaces*, 2013, **5**, 5314. (c) C. B. KC, K. Stranius, P. D'Souza, N. K. Subbaiyan, H. Lemmetyinen, N. V. Tkachenko, and F. D'Souza. *J. Phys. Chem. C*, 2013, **117**, 763.
(2) (a) B. Du, C. Stern, and P. D. Harvey. *Chem. Commun*. 2011, **47**, 6072. (b) J. Rochford, D. Chu, A. Hagfeldt, and E. Galoppini. *J. Am. Chem. Soc*., 2007, **129**, 4655.
(3) M. J. Frisch, *et al. Gaussian, Inc.*, Wallingford CT, 2004.
(4) P. Hohenberg, and W. Kohn. *Phys. Rev.*, 1964, **136**, B864.
(5) P. Hohenberg, and W. Kohn. *J. Phys. Rev.*, 1965, **140**, A1133.
(6) R. G. Parr, and W. Yang. *Density-functional theory of atoms and molecules*, Oxford Univ. Press, Oxford, 1989.
(7) D. R. Salahub, and M. C. Zerner. *The Challenge of d and f Electrons*, Amer. Chem. Soc., Washington, D.C., 1989.
(8) R. Bauernschmitt, and R. Ahlrichs. *Chem. Phys. Lett.* 1996, **256**, 454.
(9) M. E. Casida, C. Jamorski, K. C. Casida, and D. R. Salahub. *J. Chem. Phys.*, 1998, **108**, 4439.
(10) R. E. Stratmann, G. E. Scuseria, and M. J. Frisch. *J. Chem. Phys.*, 1998, **109**, 8218.
(11) C. Lee, W. Yang, and R. G. Parr. *Phys. Rev. B*, 1988, **37**, 785.
(12) B. Miehlich, A. Savin, H. Stoll, and H. Preuss. *Chem. Phys. Lett.*, 1989, **157**, 200.
(13) A. D. Becke. *J. Chem. Phys.*, 1993, **98**, 5648.
(14) J. S. Binkley, J. A. Pople, and W. J. Hehre. *J. Am. Chem. Soc.*, 1980, **102**, 939.
(15) M. S. Gordon, J. S. Binkley, J. A. Pople, W. J. Pietro, and W. J. Hehre. *J. Am. Chem. Soc.*, 1982, **104**, 2797.
(16) W. J. Pietro, M. M. Francl, W. J. Hehre, D. J. Defrees, J. A. Pople, and J. S. Binkley. *J. Am. Chem. Soc.*, 1982, **104**, 5039.
(17) K. D. Dobbs, and W. J. Hehre. *J. Comput. Chem.*, 1986, **7**, 359.
(18) K. D. Dobbs, and W. J. Hehre. *J. Comput. Chem.*, 1987, **8**, 861.
(19) K. D. Dobbs, and W. J. Hehre. *J. Comput. Chem.*, 1987, **8**, 880.

(20) N. M. O'Boyle, A. L. Tenderholt, and K. M. Langner. *J. Comp. Chem.*, 2008, **29**, 839.

Evolution of the absorption spectra upon addition of **[Pd$_3^{2+}$]** in the dye solutions

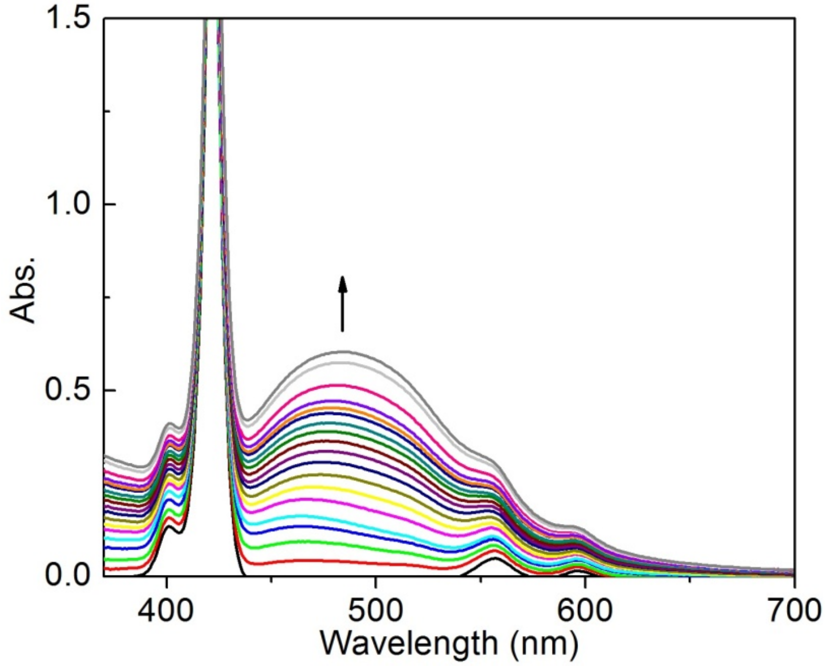

Figure S1. UV-Vis spectra for the addition of **[Pd$_3^{2+}$]** (1.21×10^{-4} M) into **MCP** (0.46×10^{-5} M) in MeOH. Curves were obtained with successive addition of 0.1 mL **[Pd$_3^{2+}$]** solution.

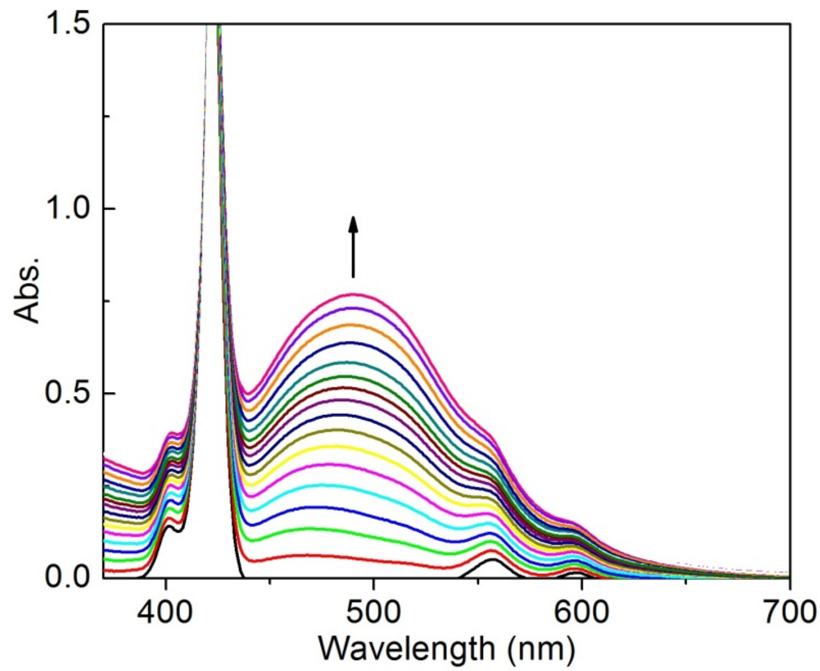

Figure S2. UV-Vis spectra for the addition of **[Pd$_3^{2+}$]** (1.18×10^{-4} M) into **DCP** (0.38×10^{-5} M) in MeOH. Curves were obtained with successive addition of 0.1 mL **[Pd$_3^{2+}$]** solution.

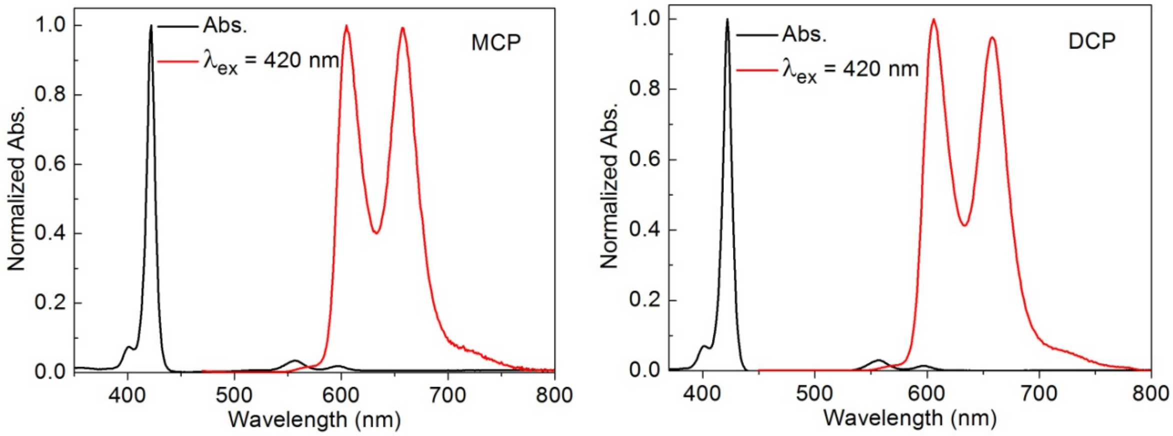

Figure S3. Absorption (black) and fluorescence (red) spectra of **MCP** (left) and **DCP** (right) in MeOH at 298 K.

Table S1. τ_F data (in ns) for **MCP** and **DCP** in MeOH at 298 K and MeOH/2MeTHF at 77 K.

[Pd_3^{2+}]/[MCP]	298 K	77 K
0	1.965±0.084	1.759±0.113
1.3	1.961±0.074	1.746±0.084
2.5	1.968±0.070	1.733±0.093
3.8	1.955±0.084	1.720±0.073
5.1	1.951±0.060	1.711±0.101
6.4	1.949±0.096	1.705±0.098
7.6	1.946±0.088	1.690±0.103
8.9	1.942±0.069	1.686±0.124

[Pd_3^{2+}]/[DCP]	298 K	77 K
0	2.041±0.097	2.403±0.113
1.2	2.042±0.075	2.504±0.108
2.3	2.040±0.074	2.545±0.095
3.3	2.039±0.074	2.538±0.098
4.2	2.037±0.074	2.525±0.095
5.0	2.036±0.074	2.555±0.284
5.8	2.036±0.074	2.545±0.095
6.5	2.037±0.077	2.354±0.080
7.1	2.031±0.073	2.345±0.085
7.7	2.032±0.073	2.325±0.195
8.3	2.027±0.109	2.315±0.095

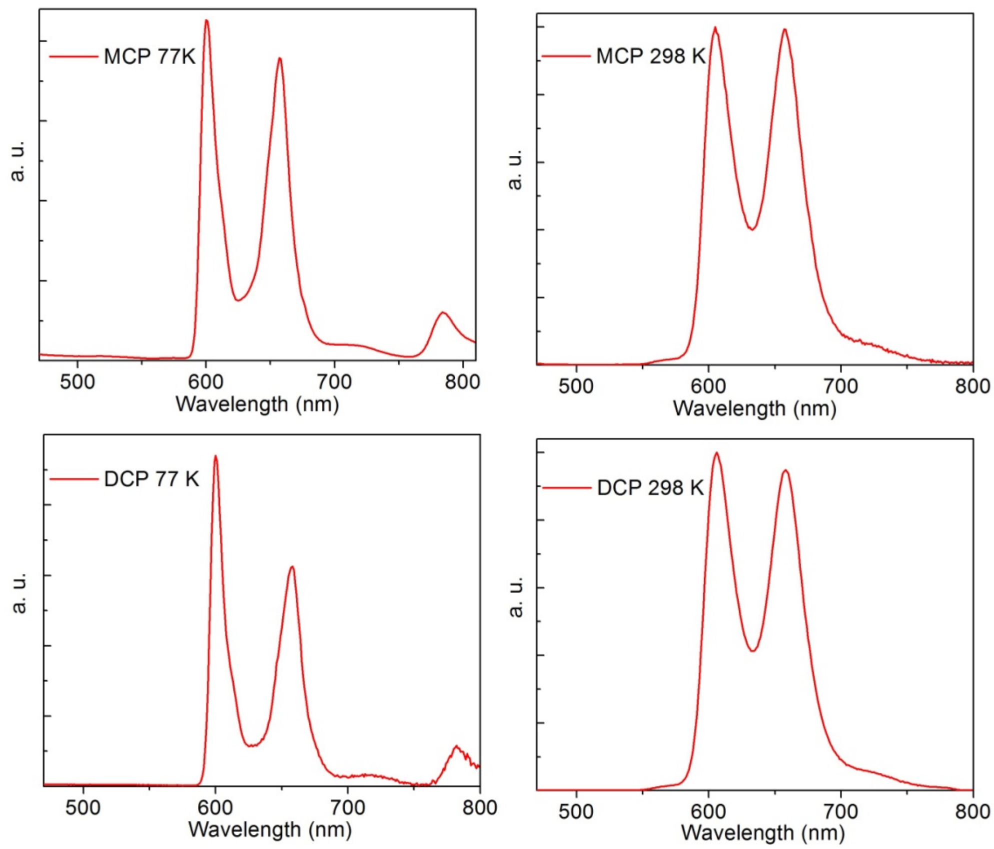

Figure S4. Comparison of the emission spectra of **MCP** and **DCP** in MeOH at 298 K (right) and MeOH/2MeTHF 1:1 at 77 K (left). Note the phosphorescence peak at about 784 nm.

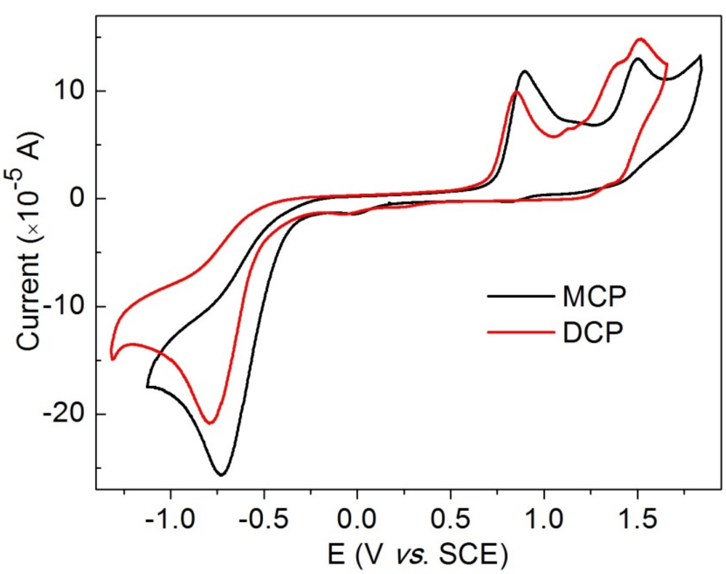

Figure S5. Cyclic voltammograms of **MCP** (black) and **DCP** (red) at a glassy carbon disk in MeOH (298 K, 1.0×10^{-3} M) containing 0.1 M $TBAPF_6$ as supporting electrolyte. (Scan rate = 50 mV/s)

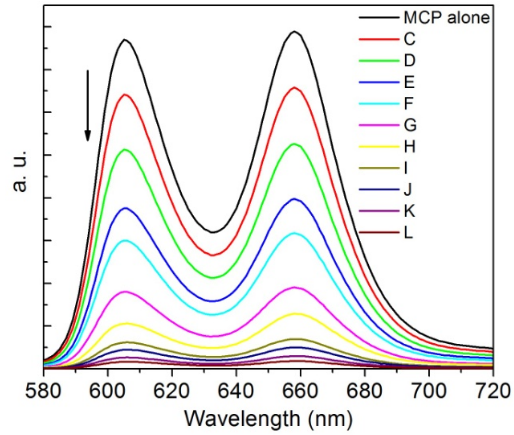

Figure S6. Variation of the fluorescence spectra of **MCP** *vs* **[Pd_3^{2+}]** in MeOH at 298 K.

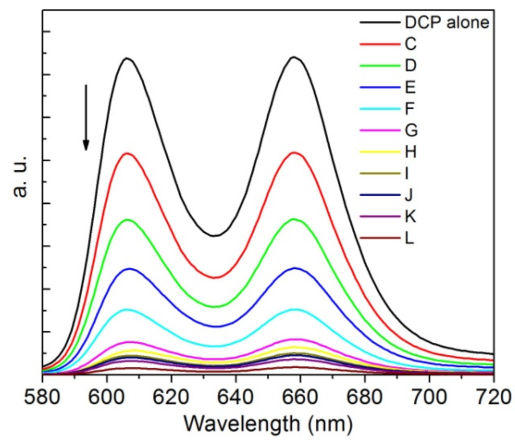

Figure S7. Variation of the fluorescence spectra of **DCP** *vs* **[Pd_3^{2+}]** in MeOH at 298 K.

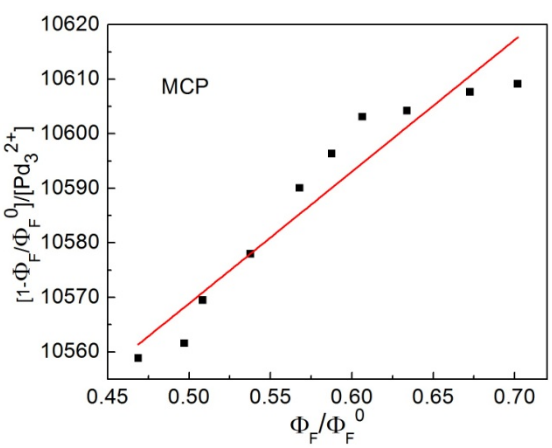

Figure S8. Graphs reporting $[1-(\Phi_F/\Phi_F°)]$/**[Pd_3^{2+}]** *vs* $\Phi_F/\Phi_F°$ for **MCP** in MeOH.

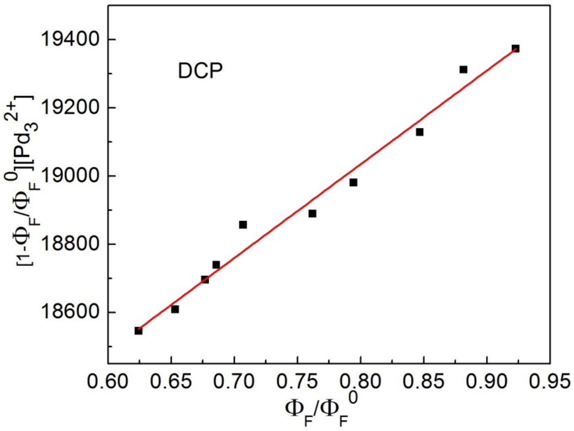

Figure S9. Graphs reporting [1-($\Phi_F/\Phi_F{}^{\circ}$)]/**[$Pd_3{}^{2+}$]** *vs* $\Phi_F/\Phi_F{}^{\circ}$ for **DCP** in MeOH.

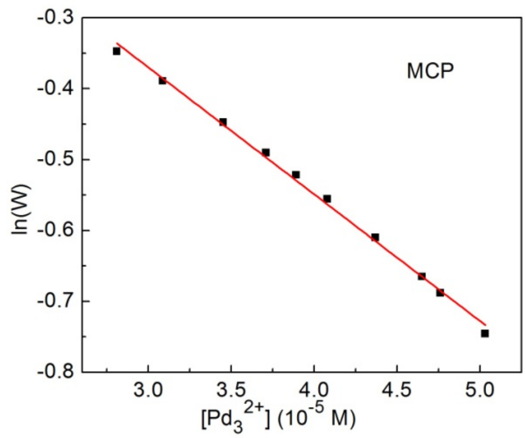

Figure S10. Graphs reporting ln(W) *vs* [$\mathbf{Pd_3{}^{2+}}$] for **MCP** in MeOH.

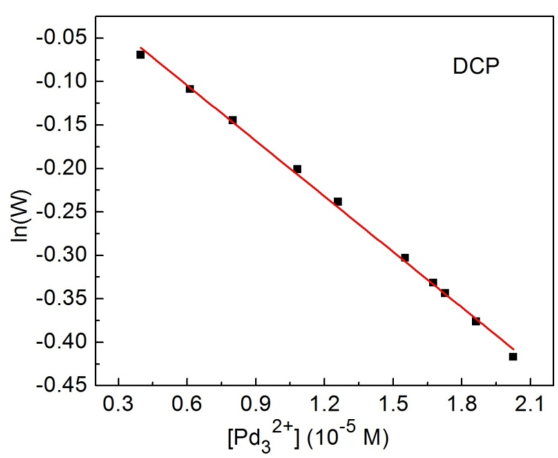

Figure S11. Graph reporting ln(W) *vs* [$\mathbf{Pd_3{}^{2+}}$] for **DCP** in MeOH at 298 K.

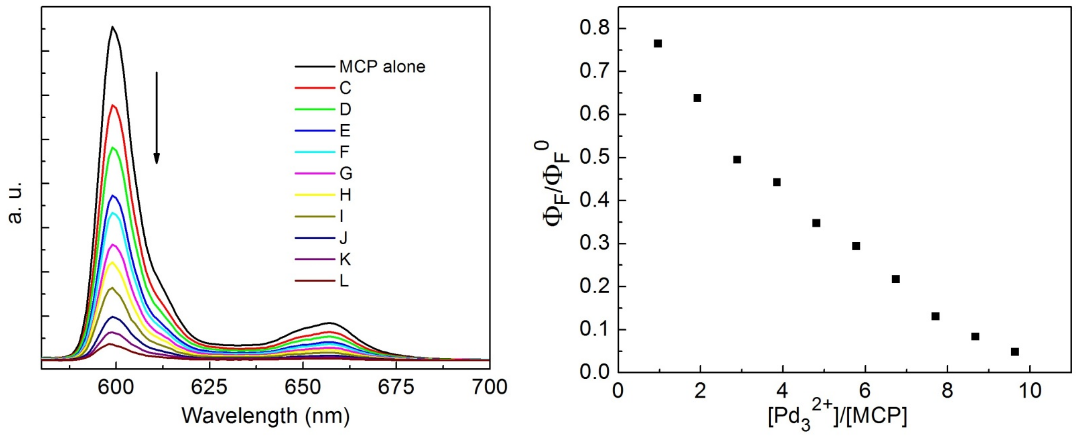

Figure S12. Left: fluorescence spectra of **MCP** (5.4×10^{-6} M) upon adding **[Pd_3^{2+}]** in MeOH/ 2MeTHF 1:1 at 77 K. Right: graphs reporting the decrease of the relative fluorescence intensity of **MCP** upon addition of **[Pd_3^{2+}]** (Φ_F and $\Phi_F°$ are the intensity in the presence and absence of **[Pd_3^{2+}]**, respectively).

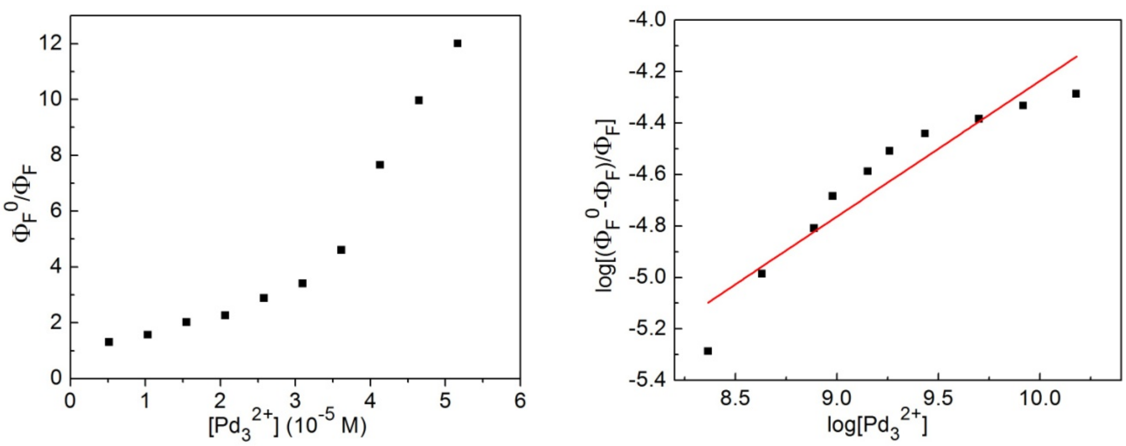

Figure S13. Left: Stern-Volmer plots of the fluorescence quenching of **MCP** in MeOH/2MeTHF 1:1 at 77 K by **[Pd_3^{2+}]** (not linear). Right: Graph reporting $\log[(\Phi_F°-\Phi_F)/\Phi_F]$ *vs* log**[Pd_3^{2+}]** (n = 0.91).

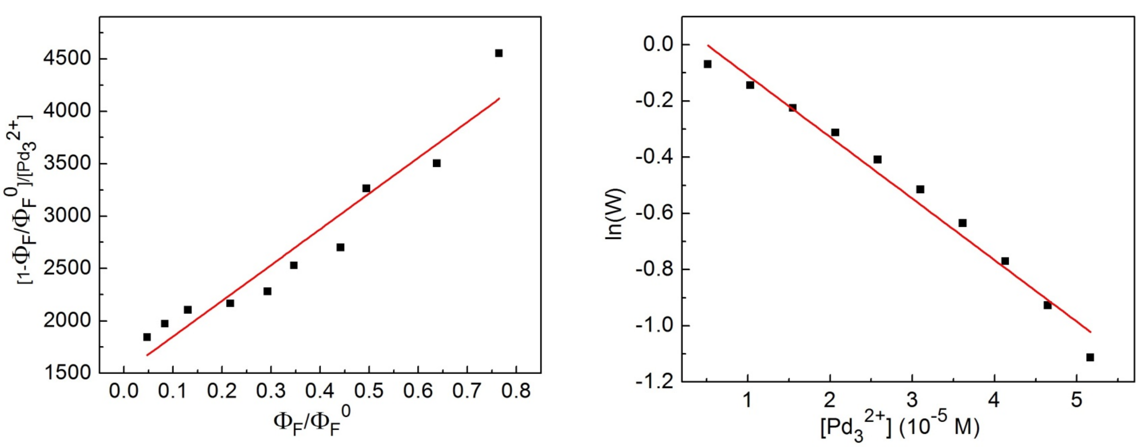

Figure S14. Graph reporting $[1-(\Phi_F/\Phi_F°)]$/**[Pd_3^{2+}]** *vs* $\Phi_F/\Phi_F°$ and ln(W) *vs* [**Pd_3^{2+}**] for **MCP** in MeOH/2MeTHF 1:1 at 77 K: dynamic constant $K_D = 3411\ M^{-1}$, static constant $V = 21913\ M^{-1}$.

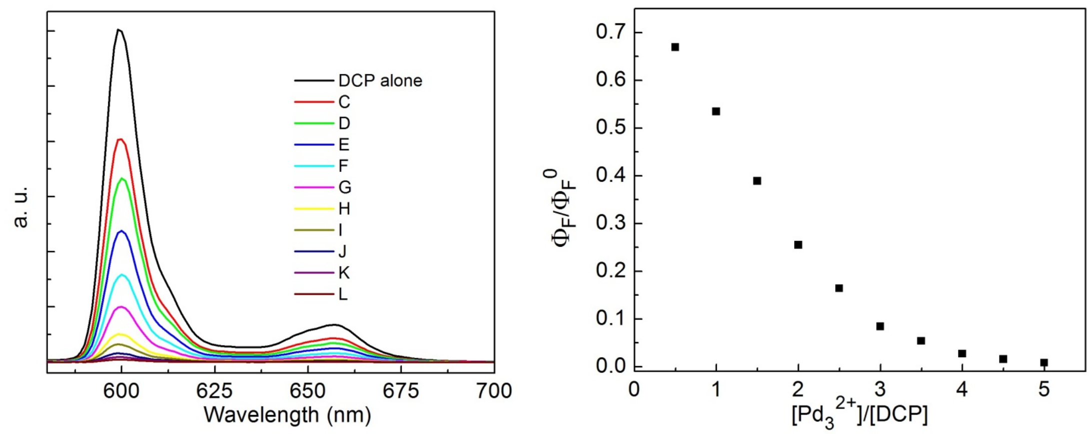

Figure S15. Left: fluorescence spectra of **DCP** (5.1×10^{-6} M) upon adding **[Pd_3^{2+}]** in MeOH/2MeTHF 1:1 at 77 K. Right: graphs reporting the decrease of the relative fluorescence intensity of **DCP** upon addition of **[Pd_3^{2+}]** (Φ_F and $\Phi_F°$ are the intensity in the presence and absence of **[Pd_3^{2+}]**, respectively).

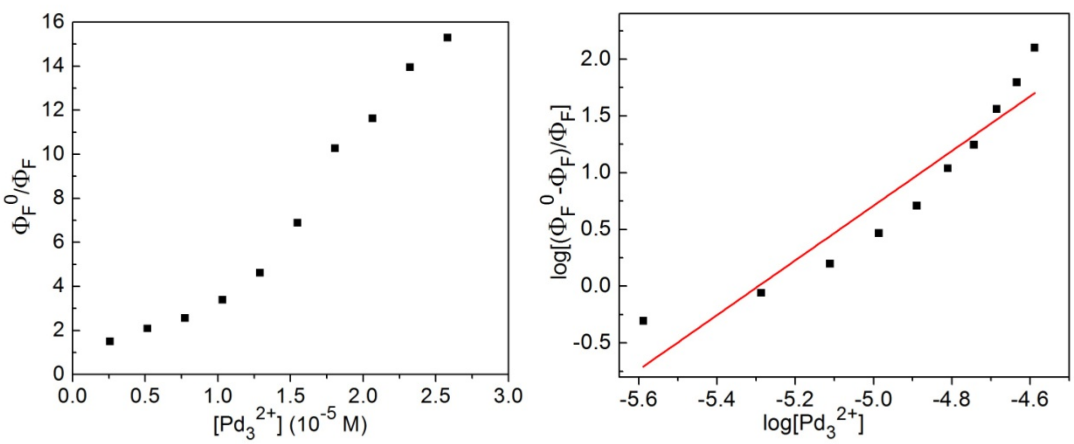

Figure S16. Left: Stern-Volmer plots of the fluorescence quenching of **DCP** in MeOH/2MeTHF 1:1 at 77 K by **[Pd_3^{2+}]** (not linear). Right: Graph reporting $\log[(\Phi_F°-\Phi_F)/\Phi_F]$ vs log**[Pd_3^{2+}]** (n = 2.20).

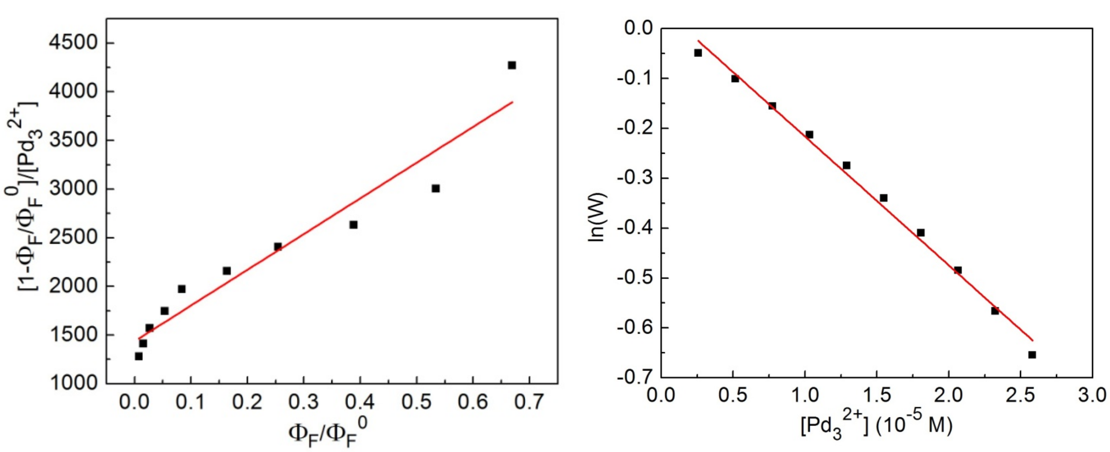

Figure S17. Graph reporting $[1-(\Phi_F/\Phi_F°)]$/**[Pd_3^{2+}]** *vs* $\Phi_F/\Phi_F°$ and ln(W) *vs* **[Pd_3^{2+}]** for **DCP** in MeOH/2MeTHF 1:1 at 77 K: dynamic constant K_D = 3673 M^{-1}, static constant V = 25819 M^{-1}.

Calculations of the relative percentage of complexed dyes

The relative percentage of complexed dyes is a function of the starting dye concentration. Here the starting concentration for calculation would be chosen as the exact concentration used for transient absorption measurements, which was favorable to elucidate the TAS. All the equations were solved by mathematical software Maple 10 from Waterloo Maplesoft Company.

(1) **[MCP]** *vs* **[Pd_3^{2+}]** = 1:1, *viz.*, **[CO_2^-]/[Pd_3^{2+}] =** 1:1

	[Pd_3^{2+}]	+	**MCP**	⇌	**[Pd_3^{2+}]•••MCP**	K_{11} = 19300 M^{-1}
Starting concentration	1.9×10^{-5}		1.9×10^{-5}		0	
Equilibrium	$1.9\times10^{-5}-x$		$1.9\times10^{-5}-x$		x	

$$\frac{x}{(1.9\times10^{-5}-x)^2}=19300$$

, $x = 4.2\times10^{-6}$, (**[Pd_3^{2+}]•••MCP**)% = $4.2\times10^{-6}/1.9\times10^{-5}$ = 22.1%

(2) **[MCP]** *vs* **[Pd_3^{2+}]** = 1:2, *viz.*, **[CO_2^-]/[Pd_3^{2+}] =** 1:2

	[Pd_3^{2+}]	+	**MCP**	⇌	**[Pd_3^{2+}]•••MCP**	K_{11} = 19300 M^{-1}
Starting concentration	1.9×10^{-5}		3.8×10^{-5}		0	
Equilibrium	$1.9\times10^{-5}-x$		$3.8\times10^{-5}-x$		x	

$$\frac{x}{(1.9\times10^{-5}-x)(3.8\times10^{-5}-x)}=19300$$

, $x = 7.1\times10^{-6}$, (**[Pd_3^{2+}]•••MCP**)% = $7.1\times10^{-6}/1.9\times10^{-5}$ = 37.4%

(3) **[MCP]** *vs* **[Pd_3^{2+}]** = 1:4, *viz.*, **[CO_2^-]/[Pd_3^{2+}] =** 1:4

	[Pd_3^{2+}]	+	**MCP**	⇌	**[Pd_3^{2+}]•••MCP**	K_{11} = 19300 M^{-1}
Starting concentration	1.9×10^{-5}		7.6×10^{-5}		0	
Equilibrium	$1.9\times10^{-5}-x$		$7.6\times10^{-5}-x$		x	

$$\frac{x}{(1.9\times10^{-5}-x)(7.6\times10^{-5}-x)}=19300$$

, $x = 10.6\times10^{-6}$, (**[Pd_3^{2+}]•••MCP**)% = $10.6\times10^{-6}/1.9\times10^{-5}$ = 55.8%

(4) **[MCP]** *vs* **[Pd_3^{2+}]** = 1:1, *viz.*, **[CO_2^-]/[Pd_3^{2+}] =** 1:1

	[Pd_3^{2+}]	+	**MCP**	⇌	**[Pd_3^{2+}]•••MCP**	V_{11} = 17900 M^{-1}
Starting concentration	1.9×10^{-5}		1.9×10^{-5}		0	
Equilibrium	$1.9\times10^{-5}-x$		$1.9\times10^{-5}-x$		x	

$$\frac{x}{(1.9\times10^{-5}-x)^2}=17900$$

, $x = 4.0\times10^{-6}$, (**[Pd_3^{2+}]•••MCP**)% = $4.0\times10^{-6}/1.9\times10^{-5}$ = 21.1%

(5) **[MCP]** *vs* **[Pd_3^{2+}]** = 1:2, *viz.*, **[CO_2^-]/[Pd_3^{2+}]** = 1:2

	[Pd_3^{2+}]	+ **MCP**	⇌ **[Pd_3^{2+}]•••MCP**	V_{11} = 17900 M^{-1}
Starting concentration	1.9×10^{-5}	3.8×10^{-5}	0	
Equilibrium	$1.9\times10^{-5}-x$	$3.8\times10^{-5}-x$	x	

$$\frac{x}{(1.9\times10^{-5}-x)(3.8\times10^{-5}-x)}=17900$$

, $x = 6.8\times10^{-6}$, (**[Pd_3^{2+}]•••MCP**)% = $6.8\times10^{-6}/1.9\times10^{-5}$ = 35.8%

(6) **[MCP]** *vs* **[Pd_3^{2+}]** = 1:4, *viz.*, **[CO_2^-]/[Pd_3^{2+}]** = 1:4

	[Pd_3^{2+}]	+ **MCP**	⇌ **[Pd_3^{2+}]•••MCP**	V_{11} = 17900 M^{-1}
Starting concentration	1.9×10^{-5}	7.6×10^{-5}	0	
Equilibrium	$1.9\times10^{-5}-x$	$7.6\times10^{-5}-x$	x	

$$\frac{x}{(1.9\times10^{-5}-x)(7.6\times10^{-5}-x)}=17900$$

, $x = 10.3\times10^{-6}$, (**[Pd_3^{2+}]•••MCP**)% = $10.3\times10^{-6}/1.9\times10^{-5}$ = 54.2%

(7) **[DCP]** *vs* **[Pd_3^{2+}]** = 1:2, *viz.*, **[CO_2^-]/[Pd_3^{2+}]** = 1:1

	[Pd_3^{2+}]	+ **DCP**	⇌ **[Pd_3^{2+}]•••DCP**	K_{12} = 21700 M^{-1}
Starting concentration	1.5×10^{-5}	3.0×10^{-5}	0	
Equilibrium	$1.5\times10^{-5}-x-y$	$3.0\times10^{-5}-2x-y$	y	

	[Pd_3^{2+}]•••DCP	+ **[Pd_3^{2+}]**	⇌ **2[Pd_3^{2+}]•••DCP**	K_{12} = 21700 M^{-1}
Starting concentration	1.5×10^{-5}	3.0×10^{-5}	0	
Equilibrium	y	$3.0\times10^{-5}-2x-y$	x	

$$\frac{y}{(1.5\times10^{-5}-x-y)\times(3.0\times10^{-5}-2x-y)}=21700\ ;\ \frac{x}{y\times(3.0\times10^{-5}-2x-y)}=21700\ ;$$

$x = 2.0\times10^{-6}$, (2**[Pd_3^{2+}]•••DCP**)% = $2.0\times10^{-6}/1.5\times10^{-5}$ = 13.3%

$y = 4.2\times10^{-6}$, (**[Pd_3^{2+}]•••DCP**)% = $4.2\times10^{-6}/1.5\times10^{-5}$ = 28.0%

(8) **[DCP]** *vs* **[Pd_3^{2+}]** = 1:4, *viz.*, **[CO_2^-]/[Pd_3^{2+}]** = 1:2

	[Pd_3^{2+}]	+ **DCP**	⇌ **[Pd_3^{2+}]•••DCP**	K_{12} = 21700 M^{-1}
Starting concentration	1.5×10^{-5}	6.0×10^{-5}	0	
Equilibrium	$1.5\times10^{-5}-x-y$	$6.0\times10^{-5}-2x-y$	y	

[Pd_3^{2+}]•••DCP + **[Pd_3^{2+}]** ⇌ **2[Pd_3^{2+}]•••DCP** K_{12} = 21700 M^{-1}

Starting concentration	1.5×10^{-5}	6.0×10^{-5}	0
Equilibrium	y	6.0×10^{-5}-2x-y	x

$$\frac{y}{(1.5\times10^{-5}-x-y)\times(6.0\times10^{-5}-2x-y)}=21700\;;\quad \frac{x}{y\times(6.0\times10^{-5}-2x-y)}=21700\;;$$

$x = 4.9\times10^{-6}$, (2**[Pd_3^{2+}]•••DCP**)% = $4.9\times10^{-6}/1.5\times10^{-5}$ = 32.7%

$y = 5.0\times10^{-6}$, (**[Pd_3^{2+}]•••DCP**)% = $5.0\times10^{-6}/1.5\times10^{-5}$ = 33.3%

(9) **[DCP]** *vs* **[Pd_3^{2+}]** = 1:8, *viz.*, **[CO_2^-]/[Pd_3^{2+}]** = 1:4

	[Pd_3^{2+}] + **DCP**	⇌	**[Pd_3^{2+}]•••DCP**	K_{12} = 21700 M^{-1}
Starting concentration	1.5×10^{-5}	12.0×10^{-5}	0	
Equilibrium	1.5×10^{-5}-x-y	12.0×10^{-5}-2x-y	y	

	[Pd_3^{2+}]•••DCP + **[Pd_3^{2+}]**	⇌	**2[Pd_3^{2+}]•••DCP**	K_{12} = 21700 M^{-1}
Starting concentration	1.5×10^{-5}	12.0×10^{-5}	0	
Equilibrium	y	12.0×10^{-5}-2x-y	x	

$$\frac{y}{(1.5\times10^{-5}-x-y)\times(12.0\times10^{-5}-2x-y)}=21700\;;$$

$$\frac{x}{y\times(12.0\times10^{-5}-2x-y)}=21700\;;$$

$x = 10.8\times10^{-6}$, (2**[Pd_3^{2+}]•••DCP**)% = $10.8\times10^{-6}/1.5\times10^{-5}$ = 72.0%

$y = 3.2\times10^{-6}$, (**[Pd_3^{2+}]•••DCP**)% = $3.2\times10^{-6}/1.5\times10^{-5}$ = 21.3%

(10) **[DCP]** *vs* **[Pd_3^{2+}]** = 1:2, *viz.*, **[CO_2^-]/[Pd_3^{2+}]** = 1:1

	[Pd_3^{2+}] + **DCP**	⇌	**[Pd_3^{2+}]•••DCP**	V_{12} = 21300 M^{-1}
Starting concentration	1.5×10^{-5}	3.0×10^{-5}	0	
Equilibrium	1.5×10^{-5}-x-y	3.0×10^{-5}-2x-y	y	

	[Pd_3^{2+}]•••DCP + **[Pd_3^{2+}]**	⇌	**2[Pd_3^{2+}]•••DCP**	V_{12} = 21300 M^{-1}
Starting concentration	1.5×10^{-5}	3.0×10^{-5}	0	
Equilibrium	y	3.0×10^{-5}-2x-y	x	

$$\frac{y}{(1.5\times10^{-5}-x-y)\times(3.0\times10^{-5}-2x-y)}=21300\;;\quad \frac{x}{y\times(3.0\times10^{-5}-2x-y)}=21300\;;$$

x = 1.9×10^{-6}, (2**[Pd$_3^{2+}$]•••DCP**)% = 1.9×10^{-6}/1.5×10^{-5} = 12.7%

y = 4.2×10^{-6}, (**[Pd$_3^{2+}$]•••DCP**)% = 4.2×10^{-6}/1.5×10^{-5} = 28.0%

(11) **[DCP]** *vs* **[Pd$_3^{2+}$]** = 1:4, *viz.*, **[CO$_2^-$]/[Pd$_3^{2+}$] =** 1:2

	[Pd$_3^{2+}$] +	**DCP** ⇌	**[Pd$_3^{2+}$]•••DCP**	V$_{12}$ = 21300 M^{-1}
Starting concentration	1.5×10^{-5}	6.0×10^{-5}	0	
Equilibrium	1.5×10^{-5}-x-y	6.0×10^{-5}-2x-y	y	

	[Pd$_3^{2+}$]•••DCP +	**[Pd$_3^{2+}$]** ⇌	**2[Pd$_3^{2+}$]•••DCP**	V$_{12}$ = 21300 M^{-1}
Starting concentration	1.5×10^{-5}	6.0×10^{-5}	0	
Equilibrium	y	6.0×10^{-5}-2x-y	x	

$$\frac{y}{\left(1.5\times 10^{-5}-x-y\right)\times\left(6.0\times 10^{-5}-2x-y\right)}=21300,\quad \frac{x}{y\times\left(6.0\times 10^{-5}-2x-y\right)}=21300;$$

x = 4.8×10^{-6}, (2**[Pd$_3^{2+}$]•••DCP**)% = 4.8×10^{-6}/1.5×10^{-5} = 32.0%

y = 5.0×10^{-6}, (**[Pd$_3^{2+}$]•••DCP**)% = 5.0×10^{-6}/1.5×10^{-5} = 33.3%

(12) **[DCP]** *vs* **[Pd$_3^{2+}$]** = 1:8, *viz.*, **[CO$_2^-$]/[Pd$_3^{2+}$] =** 1:4

	[Pd$_3^{2+}$] +	**DCP** ⇌	**[Pd$_3^{2+}$]•••DCP**	V$_{12}$ = 21300 M^{-1}
Starting concentration	1.5×10^{-5}	12.0×10^{-5}	0	
Equilibrium	1.5×10^{-5}-x-y	12.0×10^{-5}-2x-y	y	

	[Pd$_3^{2+}$]•••DCP +	**[Pd$_3^{2+}$]** ⇌	**2[Pd$_3^{2+}$]•••DCP**	V$_{12}$ = 21300 M^{-1}
Starting concentration	1.5×10^{-5}	12.0×10^{-5}	0	
Equilibrium	y	12.0×10^{-5}-2x-y	x	

$$\frac{y}{\left(1.5\times 10^{-5}-x-y\right)\times\left(12.0\times 10^{-5}-2x-y\right)}=21300;$$

$$\frac{x}{y\times\left(12.0\times 10^{-5}-2x-y\right)}=21300;$$

x = 8.8 ×10^{-6}, (2**[Pd$_3^{2+}$]•••DCP**)% = 8.8×10^{-6}/1.5×10^{-5} = 58.7%

y = 4.2 ×10^{-6}, (**[Pd$_3^{2+}$]•••DCP**)% = 4.2×10^{-6}/1.5×10^{-5} = 28.0%

<u>DFT calculation results for **MCP**</u>

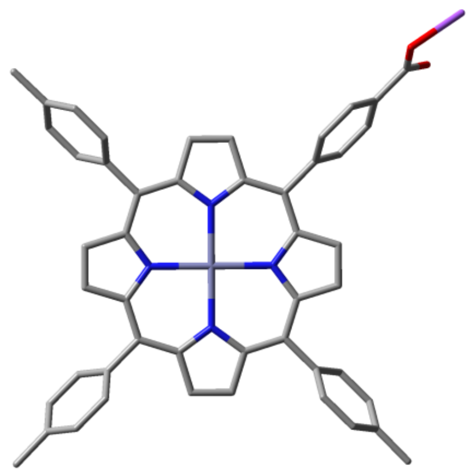

Figure S18. Optimized geometry of **MCP** (Na^+ salt) in MeOH solvent field.

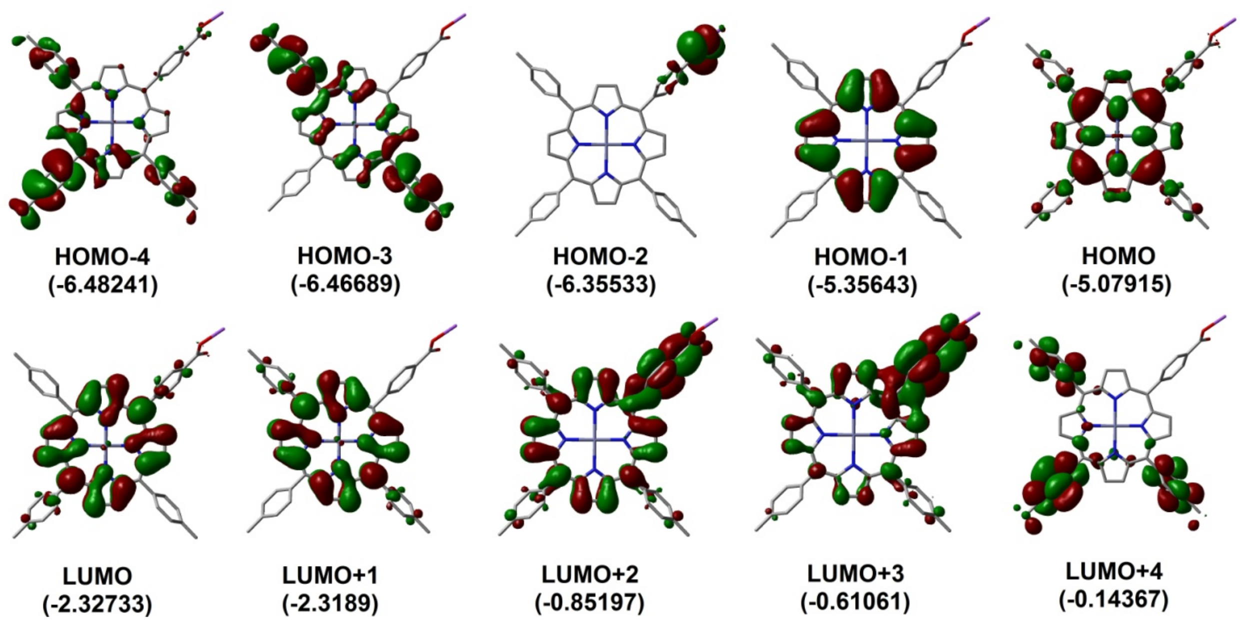

Figure S19. Representations of the frontier MOs of **MCP** (Na^+ salt) in MeOH solvent field (energies in eV).

Table S2. Computed positions and oscillator strengths for the first 100 electronic transitions for **MCP** (MeOH solvent field applied).

No.	Wavelength (nm)	Osc. Strength	Major contributions (%)
1	549	0.0564	H-1→L+1 (34), HOMO→LUMO (65)
2	548	0.0482	H-1→LUMO (35), HOMO→L+1 (64)
3	401	1.6096	H-1→L+1 (62), HOMO→LUMO (32)
4	400	1.5542	H-1→LUMO (62), HOMO→L+1 (33)
5	367	0.1084	H-6→LUMO (15), H-5→LUMO (81)
6	366	0.104	H-6→L+1 (14), H-5→L+1 (82)
7	347	0.0005	H-9→L+1 (12), H-4→L+1 (18), H-3→LUMO (39)
8	343	0	H-4→LUMO (21), H-3→L+1 (51)
9	340	0.004	H-4→LUMO (57), H-3→L+1 (35)
10	337	0.0343	H-7→LUMO (80)
11	337	0.0063	H-6→L+1 (11), H-4→L+1 (68), H-3→LUMO (10)
12	337	0.003	H-7→L+1 (61)
13	336	0.0237	H-7→L+1 (19), H-4→LUMO (11), H-2→LUMO (47)
14	335	0.0076	H-9→LUMO (14), H-8→L+1 (12), H-6→LUMO (14), H-2→LUMO (36)
15	334	0.0004	H-9→L+1 (13), H-6→L+1 (23), H-3→LUMO (43), H-2→L+1 (12)
16	331	0.0003	H-8→LUMO (10), H-2→L+1 (69)
17	331	0.0287	H-9→LUMO (14), H-6→LUMO (42), HOMO→L+2 (21)
18	329	0.0008	H-10→LUMO (17), H-8→LUMO (22), H-6→L+1 (30), H-2→L+1 (17)
19	327	0.0106	HOMO→L+2 (72)
20	325	0.0015	H-9→L+1 (64), H-8→LUMO (12)
21	321	0.0011	H-10→L+1 (18), H-9→LUMO (49), H-8→L+1 (28)
22	315	0.0009	H-16→LUMO (14), H-10→LUMO (41), H-8→LUMO (31)
23	314	0.0079	H-11→LUMO (71), HOMO→L+3 (12)
24	312	0.0115	H-11→L+1 (87)
25	310	0.0023	H-10→L+1 (28), H-8→L+1 (26), HOMO→L+3 (29)
26	308	0.0036	H-11→LUMO (15), H-10→L+1 (14), HOMO→L+3 (51)
27	307	0.0006	H-13→L+1 (91)
28	307	0.0008	H-14→LUMO (80)
29	306	0.0002	H-15→L+1 (81)
30	303	0.001	H-1→L+2 (84)
31	302	0.0023	H-13→LUMO (93)
32	301	0.0003	H-14→L+1 (85)
33	301	0	H-15→LUMO (83)
34	299	0.0248	H-17→L+1 (15), H-16→LUMO (54), H-10→LUMO (10)
35	298	0.0028	H-12→LUMO (93)
36	297	0.1949	H-17→LUMO (84)
37	297	0.1831	H-17→L+1 (68), H-16→LUMO (15)
38	295	0.0004	H-16→L+1 (79)
39	294	0	H-12→L+1 (99)

40	289	0.026	H-1→L+3 (94)
41	280	0.0135	HOMO→L+4 (98)
42	278	0.0341	HOMO→L+5 (97)
43	276	0.001	HOMO→L+6 (93)
44	276	0.0091	HOMO→L+7 (67), HOMO→L+9 (25)
45	274	0.0035	HOMO→L+8 (96)
46	274	0.0037	HOMO→L+7 (26), HOMO→L+9 (69)
47	273	0	H-2→L+2 (44), H-2→L+3 (49)
48	271	0.0047	HOMO→L+10 (35), HOMO→L+11 (61)
49	267	0	H-19→L+1 (47), H-18→LUMO (50)
50	263	0.0092	H-1→L+4 (97)
51	262	0.0265	H-1→L+5 (94)
52	261	0	H-19→LUMO (43), H-18→L+1 (43), H-1→L+6 (11)
53	259	0.0057	H-1→L+7 (58), H-1→L+9 (37)
54	259	0.0001	H-1→L+6 (85)
55	258	0.0001	H-1→L+8 (93)
56	257	0.0016	H-1→L+7 (39), H-1→L+9 (58)
57	257	0	HOMO→L+10 (63), HOMO→L+11 (37)
58	254	0.001	H-1→L+10 (36), H-1→L+11 (62)
59	251	0	H-6→L+2 (12), H-5→L+2 (64)
60	249	0.0043	H-19→L+1 (45), H-18→LUMO (41)
61	247	0	H-12→L+2 (45), H-12→L+3 (50)
62	244	0.0044	H-19→LUMO (42), H-18→L+1 (43)
63	243	0.0002	H-1→L+10 (63), H-1→L+11 (37)
64	240	0.0024	H-8→L+2 (11), H-7→L+2 (40)
65	240	0	H-3→L+2 (87)
66	239	0.001	H-4→L+2 (78)
67	237	0.0004	H-8→L+2 (21), H-7→L+2 (44)
68	237	0.0002	H-6→L+2 (57), H-5→L+2 (12), H-4→L+2 (11)
69	234	0.0581	H-10→L+2 (56), H-8→L+2 (25)
70	234	0	H-2→L+2 (48), H-2→L+3 (45)
71	233	0.1009	H-9→L+2 (72), H-6→L+2 (10)
72	232	0	HOMO→L+14 (95)
73	231	0.0139	H-16→L+2 (14), H-16→L+3 (12), H-8→L+2 (14), H-2→L+10 (16), H-2→L+11 (10)
74	230	0.0019	H-4→L+6 (11)
75	230	0.0001	H-3→L+6 (19)
76	230	0.0008	H-14→L+4 (11), H-4→L+8 (17)
77	229	0.0002	H-5→L+2 (14), H-5→L+3 (58)
78	228	0.0058	H-10→L+3 (14), H-7→L+3 (33), H-3→L+3 (40)
79	227	0.0617	H-11→L+2 (37), H-9→L+3 (11), H-6→L+3 (32)
80	227	0.0067	H-22→LUMO (13), HOMO→L+15 (11), HOMO→L+16 (46), HOMO→L+17 (21)

81	226	0.0002	H-22→LUMO (48), H-21→L+1 (47)
82	226	0.2069	H-11→L+2 (46), H-6→L+3 (17)
83	225	0.0095	H-7→L+3 (20), H-3→L+3 (40)
84	225	0.0083	H-22→L+1 (49), H-21→LUMO (46)
85	224	0.0001	H-22→LUMO (35), H-21→L+1 (46)
86	224	0.0039	H-10→L+2 (10), H-10→L+3 (10), H-3→L+3 (10), H-2→L+10 (38)
87	223	0.0003	H-2→L+10 (14), H-2→L+11 (64)
88	223	0.0257	H-9→L+3 (10), H-6→L+3 (17), H-5→L+3 (11), H-4→L+3 (40)
89	222	0.017	H-22→L+1 (39), H-21→LUMO (31), H-6→L+3 (11)
90	221	0.0088	H-16→L+2 (11), H-14→L+2 (10), H-10→L+3 (22), H-8→L+3 (18), H-2→L+10 (14), H-2→L+11 (10)
91	221	0.0047	H-13→L+2 (30), H-9→L+3 (27), H-4→L+3 (17)
92	221	0.0005	H-1→L+14 (93)
93	221	0.0102	H-13→L+2 (53), H-9→L+3 (11)
94	220	0.0021	H-16→L+2 (14), H-15→L+2 (13), H-14→L+2 (46)
95	220	0.0045	H-15→L+2 (60), H-14→L+2 (20)
96	218	0.0006	HOMO→L+12 (95)
97	218	0.0004	H-10→L+3 (25), H-8→L+3 (41), H-7→L+3 (19)
98	218	0	HOMO→L+13 (99)
99	217	0.0381	H-20→LUMO (31), H-17→L+2 (47)
100	217	0.1111	H-20→L+1 (92)

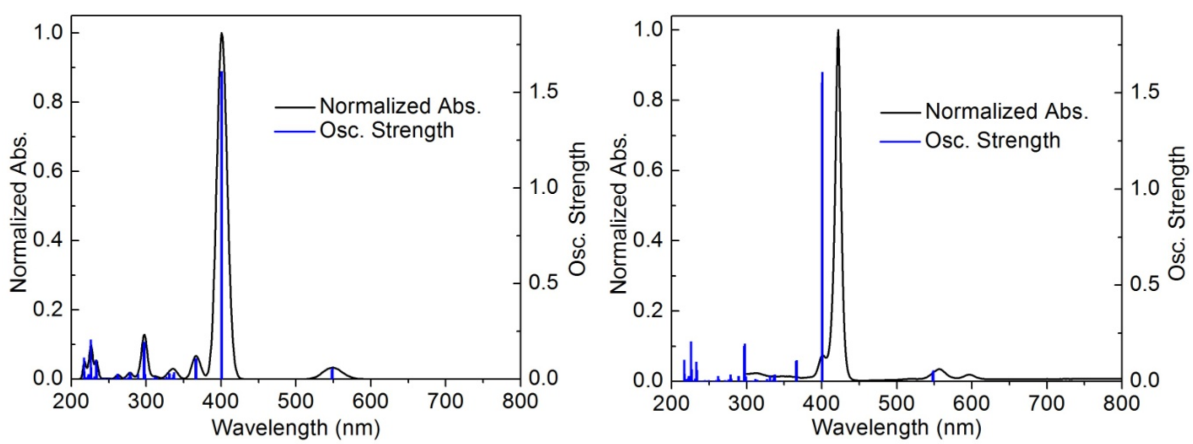

Figure S20. Left: Computed positions and oscillator strength for the 100st electronic transitions for **MCP** (MeOH solvent field applied). The black line is generated by applying a thickness of 500 cm^{-1}. Right: Experimental UV-vis spectrum (in MeOH) and oscillator strength for the 100st electronic transitions for **MCP** (MeOH solvent field applied).

DFT calculation results for DCP

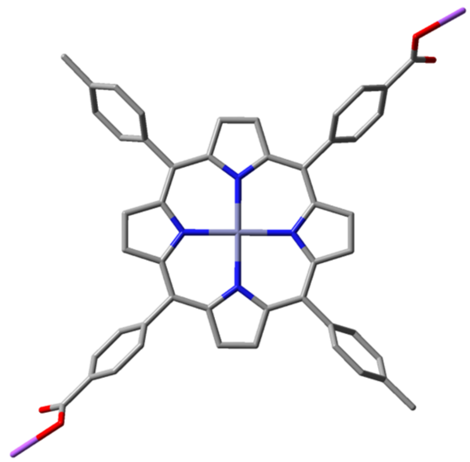

Figure S21. Optimized geometry of **DCP** (Na^+ salt) in MeOH solvent field.

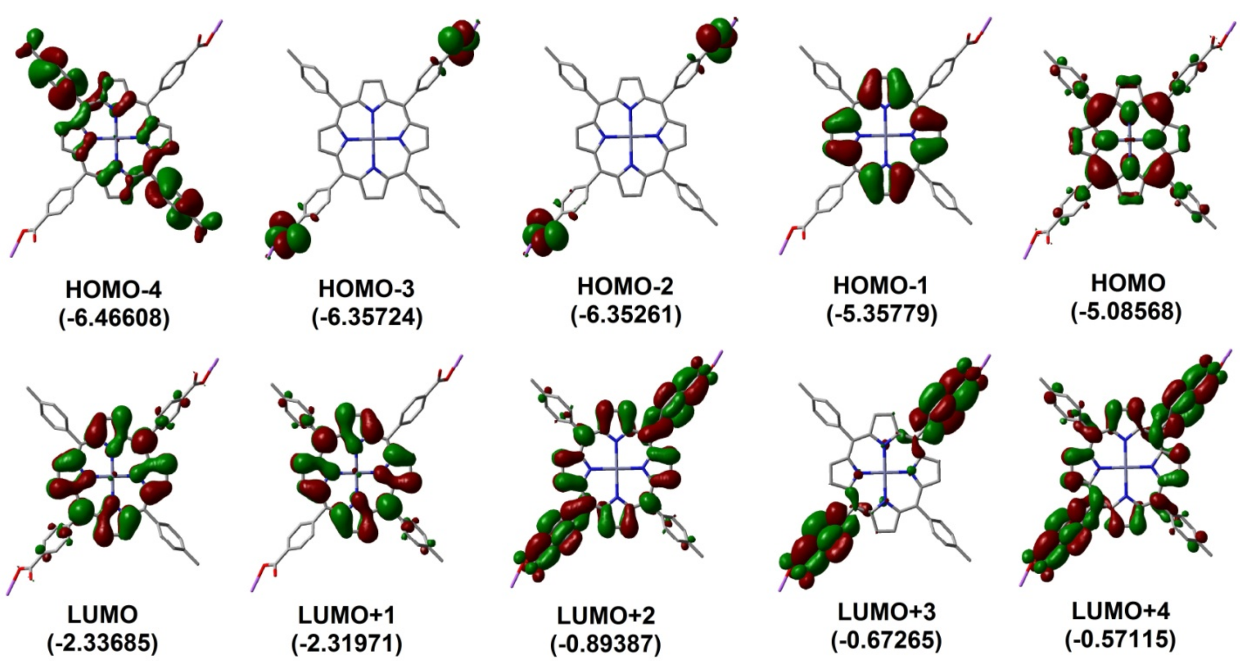

Figure S22. Representations of the frontier MOs of **DCP** (Na^+ salt) in MeOH solvent field (energies in eV).

Table S3. Computed positions and oscillator strengths for the first 100 electronic transitions for **DCP** (MeOH solvent field applied).

No.	Wavelength (nm)	Osc. Strength	Major contributions (%)
1	549	0.0616	H-1→L+1 (34), HOMO→LUMO (66)
2	547	0.0452	H-1→LUMO (36), HOMO→L+1 (64)
3	401	1.666	H-1→L+1 (63), HOMO→LUMO (32)
4	401	1.5557	H-1→LUMO (61), HOMO→L+1 (34)
5	367	0.1121	H-6→LUMO (38), H-5→LUMO (58)
6	366	0.1032	H-6→L+1 (35), H-5→L+1 (61)
7	347	0	H-12→LUMO (11), H-7→L+1 (24), H-4→LUMO (44)
8	343	0	H-7→LUMO (15), H-4→L+1 (63)
9	338	0	H-7→LUMO (18), H-4→L+1 (28), H-2→LUMO (40)
10	338	0.0329	H-10→LUMO (10), H-8→LUMO (82)
11	337	0.005	H-8→L+1 (62), H-3→LUMO (16)
12	337	0.0062	H-8→L+1 (14), H-3→LUMO (81)
13	336	0	H-7→LUMO (16), H-2→LUMO (55)
14	335	0.0002	H-11→L+1 (12), H-7→L+1 (20), H-4→LUMO (50), H-2→L+1 (12)
15	334	0.0035	H-6→L+1 (49), H-5→L+1 (31), H-3→L+1 (15)
16	333	0.0857	H-6→LUMO (56), H-5→LUMO (33)
17	332	0	H-7→LUMO (15), HOMO→L+2 (74)
18	332	0	H-12→LUMO (10), H-9→LUMO (11), H-2→L+1 (72)
19	331	0.0009	H-3→L+1 (85)
20	329	0	H-12→LUMO (21), H-9→LUMO (30), H-7→L+1 (31), H-2→L+1 (13)
21	327	0	H-12→L+1 (15), H-11→LUMO (19), H-7→LUMO (33), HOMO→L+2 (20)
22	322	0.0003	H-11→L+1 (71), H-7→L+1 (21)
23	321	0	H-12→L+1 (16), H-11→LUMO (52), H-9→L+1 (27)
24	316	0.0003	H-18→LUMO (18), H-12→LUMO (40), H-9→LUMO (39)
25	316	0.0137	H-13→LUMO (35), HOMO→L+3 (62)
26	315	0.0029	H-19→LUMO (17), H-10→LUMO (70), H-8→LUMO (10)
27	311	0.0036	H-13→LUMO (24), H-10→L+1 (35), H-8→L+1 (13), HOMO→L+3 (15)
28	311	0	H-18→L+1 (10), H-12→L+1 (41), H-9→L+1 (46)
29	309	0.0058	H-13→L+1 (86)
30	308	0.0063	H-13→LUMO (26), H-10→L+1 (42), HOMO→L+3 (19)
31	308	0.0004	H-16→L+1 (66), H-1→L+2 (29)
32	307	0	H-16→LUMO (12), HOMO→L+4 (83)
33	306	0.0007	H-17→L+1 (89)
34	306	0.0006	H-16→L+1 (31), H-1→L+2 (62)
35	303	0	H-16→LUMO (85), HOMO→L+4 (12)
36	302	0	H-17→LUMO (92)
37	299	0.0021	H-18→LUMO (78), H-12→LUMO (11)
38	299	0.0219	H-20→L+1 (20), H-19→LUMO (55), H-10→LUMO (17)

39	298	0.002	H-15→LUMO (87)
40	298	0.0001	H-14→LUMO (92)
41	297	0.1809	H-20→LUMO (82)
42	297	0.0951	H-20→L+1 (51), H-19→LUMO (18), H-1→L+3 (16)
43	295	0	H-18→L+1 (87)
44	294	0.0005	H-19→L+1 (80)
45	294	0	H-14→L+1 (98)
46	294	0	H-15→L+1 (95)
47	293	0.1391	H-20→L+1 (15), H-1→L+3 (80)
48	287	0.0011	H-1→L+4 (94)
49	277	0.0315	HOMO→L+5 (97)
50	277	0.0001	HOMO→L+7 (96)
51	275	0.0018	HOMO→L+6 (97)
52	274	0.0154	HOMO→L+8 (95)
53	273	0	H-3→L+3 (37), H-2→L+2 (29), H-2→L+4 (17)
54	273	0	H-3→L+2 (29), H-3→L+4 (18), H-2→L+3 (38)
55	271	0.0022	HOMO→L+9 (96)
56	270	0.0076	HOMO→L+12 (90)
57	267	0.0001	H-22→L+1 (46), H-21→LUMO (52)
58	262	0.0269	H-1→L+5 (98)
59	261	0.0001	H-22→LUMO (45), H-21→L+1 (44)
60	261	0.0003	H-1→L+7 (95)
61	258	0	H-1→L+6 (90)
62	257	0.0051	H-1→L+8 (98)
63	257	0	HOMO→L+10 (12), HOMO→L+11 (87)
64	257	0	HOMO→L+10 (81), HOMO→L+11 (12)
65	255	0	H-1→L+9 (97)
66	254	0.0013	H-1→L+12 (92)
67	252	0	H-6→L+2 (30), H-5→L+2 (47)
68	249	0.0041	H-22→L+1 (47), H-21→LUMO (39)
69	247	0	H-15→L+3 (36), H-14→L+2 (31), H-14→L+4 (18)→
70	247	0	H-15→L+2 (31), H-15→L+4 (18), H-14→L+3 (36)
71	245	0	H-22→LUMO (41), H-21→L+1 (43)
72	243	0.0001	H-1→L+10 (25), H-1→L+11 (73)
73	243	0.0003	H-1→L+10 (68), H-1→L+11 (26)
74	241	0.0002	H-4→L+2 (89)
75	241	0.0027	H-9→L+3 (13), H-8→L+2 (58)
76	240	0.0032	H-9→L+2 (34), H-8→L+3 (15)
77	239	0.0043	H-11→L+2 (13), H-7→L+2 (70)
78	237	0.0003	H-10→L+2 (31), H-8→L+2 (23)
79	237	0	H-6→L+2 (51), H-5→L+2 (36)
80	236	0	H-3→L+2 (61), H-3→L+4 (16), H-2→L+3 (17)
81	236	0	H-3→L+3 (16), H-2→L+2 (56), H-2→L+4 (16)

82	235	0.0443	H-12→L+2 (64), H-9→L+2 (11)
83	233	0.1786	H-11→L+2 (73), H-7→L+2 (14)
84	232	0	HOMO→L+17 (94)
85	231	0.0143	H-19→L+2 (10), H-18→L+3 (13), H-10→L+2 (20), H-3→L+11 (12), H-2→L+10 (11)
86	231	0.0109	H-19→L+3 (11), H-18→L+2 (13), H-10→L+3 (10), H-9→L+2 (17), H-3→L+10 (11), H-2→L+11 (12)
87	230	0.0019	H-17→L+7 (11), H-16→L+5 (13), H-5→L+6 (10), H-4→L+8 (24)
88	230	0.0008	H-5→L+3 (22), H-4→L+6 (17)
89	229	0	H-6→L+3 (30), H-5→L+3 (43)
90	229	0	H-6→L+4 (20), H-5→L+2 (10), H-5→L+4 (41)
91	229	0	H-8→L+4 (18), H-4→L+3 (56)
92	228	0.0136	H-9→L+4 (12), H-8→L+3 (39), H-4→L+4 (19)
93	227	0	H-13→L+2 (16), H-11→L+3 (15), H-7→L+3 (45)
94	226	0.0045	H-25→LUMO (39), HOMO→L+18 (10), HOMO→L+20 (24), HOMO→L+21 (12)
95	226	0.0021	H-25→LUMO (27), H-24→L+1 (47), HOMO→L+20 (12)
96	226	0.5141	H-7→L+4 (50), H-6→L+3 (20)
97	226	0	H-13→L+2 (65), H-7→L+3 (13)
98	226	0.0001	H-10→L+2 (20), H-8→L+4 (13), H-4→L+3 (23)
99	225	0.0027	H-12→L+2 (15), H-9→L+2 (21), H-4→L+4 (25)
100	225	0	H-25→L+1 (49), H-24→LUMO (42)

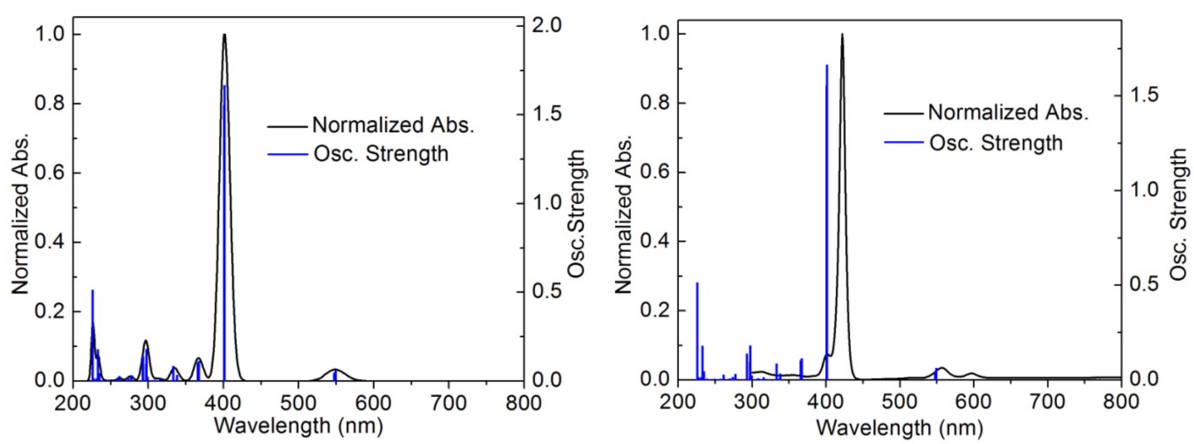

Figure S23. Left: Computed positions and oscillator strength for the 100st electronic transitions for **DCP** (MeOH solvent field applied). The black line is generated by applying a thickness of 500 cm^{-1}. Right: Experimental UV-vis spectrum (in MeOH) and oscillator strength for the 100st electronic transitions for **DCP** (MeOH solvent field applied).

DFT calculation results for $[Pd_3^{2+}]$

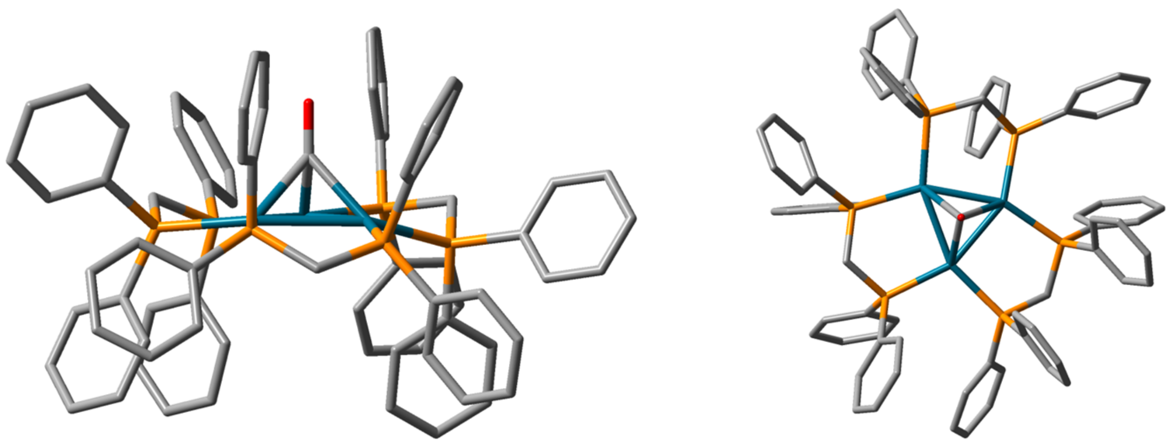

Side View Top View

Figure S24. Optimized geometry of **$[Pd_3^{2+}]$** in MeOH solvent field. The computed Pd-Pd distances are 2.685 Å, 2.679 Å, and 2.649 Å.

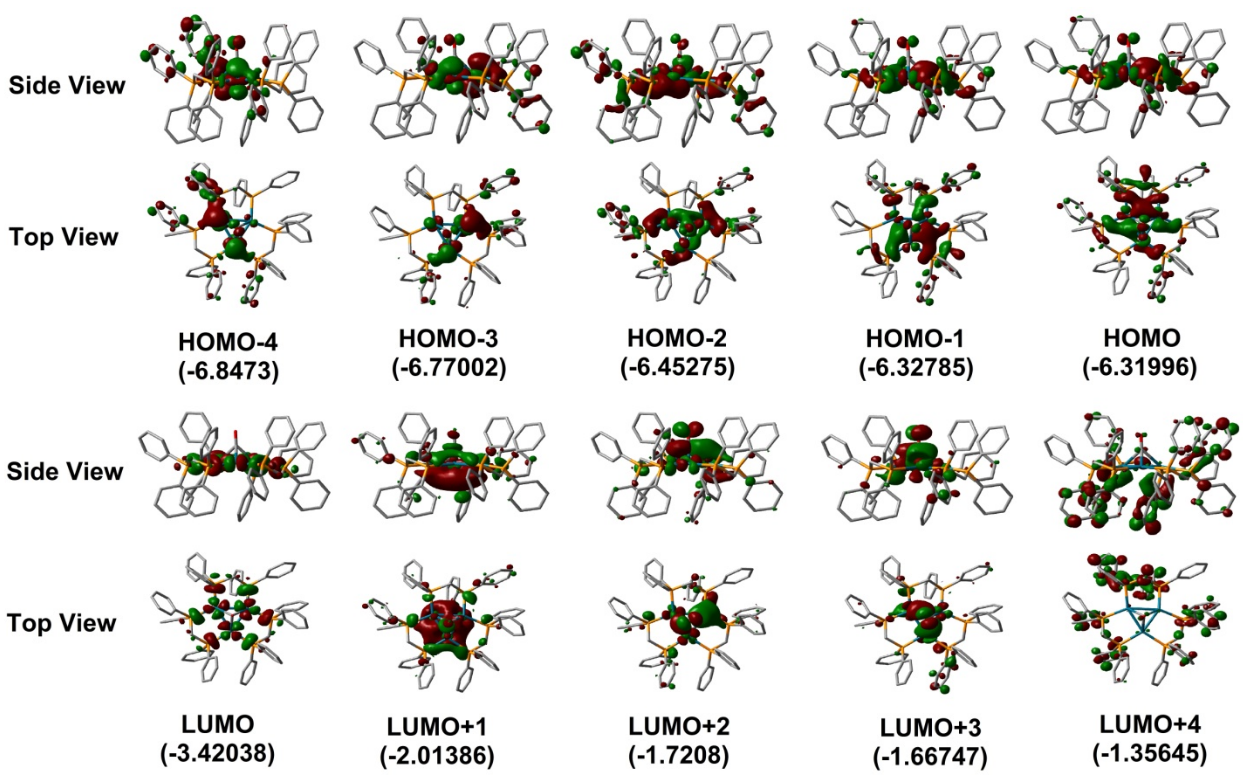

Figure S25. Representations of the frontier MOs of **$[Pd_3^{2+}]$** in MeOH solvent field (energies in eV).

Table S4. Computed positions and oscillator strengths for the first 100 electronic transitions for **[Pd_3^{2+}]** (MeOH solvent field applied).

No.	Wavelength (nm)	Osc. Strength	Major contributions (%)
1	605	0.0062	H-2→LUMO (71), HOMO→LUMO (22)
2	544	0.0668	H-3→LUMO (56), HOMO→LUMO (21)
3	522	0.1267	H-4→LUMO (35), H-3→LUMO (12), H-1→LUMO (44)
4	499	0.269	H-4→LUMO (30), H-3→LUMO (16), H-1→LUMO (11), HOMO→LUMO (29)
5	495	0.3364	H-4→LUMO (22), H-2→LUMO (14), H-1→LUMO (27), HOMO→LUMO (23)
6	421	0.012	H-26→LUMO (10), H-19→LUMO (11), H-15→LUMO (14), H-14→LUMO (23)
7	418	0.0113	H-23→LUMO (25), H-19→LUMO (17)
8	413	0.0115	H-24→LUMO (20), H-21→LUMO (18)
9	397	0.0022	H-32→LUMO (15), H-26→LUMO (13), H-19→LUMO (14)
10	387	0.0017	H-33→LUMO (32), H-25→LUMO (14)
11	381	0.0052	H-34→LUMO (34), H-23→LUMO (13)
12	374	0.0002	H-5→LUMO (83)
13	366	0.0001	H-6→LUMO (69)
14	365	0.0001	H-10→LUMO (28), H-8→LUMO (43), H-7→LUMO (11)
15	364	0.0002	H-8→LUMO (31), H-7→LUMO (37), H-6→LUMO (19)
16	361	0.0002	H-10→LUMO (47), H-8→LUMO (13), H-7→LUMO (23)
17	361	0.0009	H-9→LUMO (58)
18	357	0.0006	H-11→LUMO (74)
19	355	0.0009	H-12→LUMO (75)
20	351	0.0016	H-13→LUMO (62), HOMO→L+1 (15)
21	350	0.0067	H-13→LUMO (10), H-1→L+1 (12), HOMO→L+1 (63)
22	349	0.0204	H-1→L+1 (76)
23	346	0.0016	H-16→LUMO (14), H-15→LUMO (47)
24	343	0.0021	H-17→LUMO (12), H-16→LUMO (22), H-14→LUMO (24)
25	342	0.0012	H-18→LUMO (12), H-16→LUMO (17), H-14→LUMO (14)
26	341	0.0004	H-17→LUMO (66)
27	339	0.003	H-20→LUMO (18), H-18→LUMO (36), H-2→L+1 (10)
28	338	0.0156	H-2→L+1 (60)
29	336	0.0059	H-23→LUMO (15), H-22→LUMO (15), H-20→LUMO (34)
30	335	0.0003	H-25→LUMO (28), H-19→LUMO (28)
31	333	0.0042	H-25→LUMO (11), H-23→LUMO (11), H-22→LUMO (12), H-21→LUMO (13)
32	331	0.0036	H-27→LUMO (14), H-1→L+2 (15), HOMO→L+2 (30)
33	331	0.0073	H-35→LUMO (20), H-28→LUMO (31), H-1→L+2 (12)
34	330	0.0081	H-24→LUMO (21), H-21→LUMO (18)
35	327	0.023	H-27→LUMO (12), H-26→LUMO (26), H-25→LUMO (16)

36	327	0.0275	H-29→LUMO (13), H-22→LUMO (18)
37	324	0.0237	H-1→L+2 (18), H-1→L+3 (17), HOMO→L+2 (26)
38	322	0.0625	H-30→LUMO (15), H-1→L+2 (15), HOMO→L+3 (14)
39	320	0.0485	H-30→LUMO (28), H-29→LUMO (22), HOMO→L+3 (17)
40	320	0.0055	H-32→LUMO (22), H-2→L+3 (16)
41	318	0.006	H-32→LUMO (19), H-3→L+1 (32), H-1→L+3 (10)
42	317	0.0096	H-31→LUMO (42), H-3→L+1 (22)
43	315	0.0043	H-35→LUMO (28), H-28→LUMO (14)
44	314	0.0159	H-36→LUMO (19), H-32→LUMO (12), H-31→LUMO (23), H-2→L+3 (12)
45	311	0.0533	H-35→LUMO (10), H-1→L+3 (26), HOMO→L+3 (20)
46	309	0.0104	H-4→L+1 (64)
47	306	0.313	H-3→L+1 (12), H-2→L+2 (38), H-2→L+3 (16)
48	304	0.3167	H-36→LUMO (10), H-4→L+1 (16), H-2→L+2 (18), H-2→L+3 (29)
49	298	0.0124	H-3→L+2 (76)
50	294	0.0166	H-3→L+3 (77)
51	291	0.032	H-4→L+2 (78)
52	286	0.0164	H-4→L+3 (77)
53	283	0.0034	HOMO→L+4 (79)
54	281	0.0177	H-1→L+4 (86)
55	280	0.0065	H-1→L+5 (47), HOMO→L+5 (39)
56	278	0.0094	H-1→L+5 (31), HOMO→L+5 (44)
57	276	0.013	H-1→L+5 (10), H-1→L+6 (65)
58	275	0.0133	H-2→L+4 (14), HOMO→L+6 (54)
59	274	0.0138	H-2→L+4 (52), HOMO→L+6 (21)
60	273	0.0165	H-24→L+1 (13), H-14→L+1 (10), H-5→L+1 (12)
61	272	0.0075	H-2→L+4 (18), H-2→L+5 (62)
62	270	0.0932	H-21→L+1 (14), H-15→L+1 (12)
63	269	0.1083	H-38→LUMO (17), H-14→L+1 (17)
64	268	0.0383	H-2→L+6 (34), HOMO→L+7 (34)
65	268	0.1501	H-23→L+1 (15), H-19→L+1 (23), HOMO→L+7 (13)
66	267	0.0308	H-2→L+6 (43), H-1→L+7 (10), HOMO→L+7 (22)
67	265	0.0081	H-1→L+7 (48), HOMO→L+8 (29)
68	264	0.0076	H-5→L+1 (64)
69	263	0.0009	H-1→L+7 (18), H-1→L+9 (27), HOMO→L+8 (29)
70	263	0.0067	H-1→L+8 (39), H-1→L+9 (38)
71	262	0.0137	H-7→L+1 (24), H-1→L+8 (10)
72	261	0.0161	H-1→L+8 (33), H-1→L+9 (17), HOMO→L+9 (10)
73	260	0.0005	H-2→L+7 (10), HOMO→L+9 (50)
74	260	0.0145	H-10→L+1 (10)
75	260	0.0142	H-2→L+7 (43)
76	259	0.0132	H-6→L+1 (27), HOMO→L+10 (37)
77	259	0.0059	H-9→L+1 (15), H-2→L+8 (15)

78	258	0.0241	H-8→L+1 (12), H-6→L+1 (16), HOMO→L+10 (34)
79	258	0.0287	H-8→L+1 (12), H-2→L+8 (12), H-1→L+10 (12)
80	258	0.0124	H-9→L+1 (13), H-8→L+1 (25), H-2→L+8 (13)
81	258	0.0328	H-1→L+10 (59)
82	258	0.0079	H-8→L+1 (12), H-7→L+1 (31), H-6→L+1 (17)
83	257	0.0055	H-10→L+1 (10)
84	256	0.0096	H-3→L+4 (18)
85	256	0.0274	H-11→L+1 (11), H-2→L+8 (12)
86	256	0.0027	H-11→L+1 (17), H-10→L+1 (23), H-8→L+1 (13)
87	255	0.0084	HOMO→L+11 (54)
88	255	0.0095	H-12→L+1 (22), H-11→L+1 (12)
89	254	0.0143	H-9→L+1 (16)
90	254	0.0392	H-3→L+4 (15), H-2→L+9 (10), H-1→L+11 (13)
91	254	0.0323	HOMO→L+11 (10)
92	253	0.12	H-2→L+10 (12), H-1→L+11 (11)
93	253	0.0481	H-12→L+1 (12)
94	253	0.0157	H-1→L+11 (43), H-1→L+12 (10)
95	252	0.0145	H-12→L+1 (11)
96	252	0.0035	H-3→L+5 (22), H-2→L+9 (40)
97	252	0.0277	H-1→L+12 (27), HOMO→L+12 (16)
98	251	0.0268	
99	251	0.009	H-13→L+1 (40)
100	251	0.0169	H-13→L+1 (10), H-2→L+10 (30)

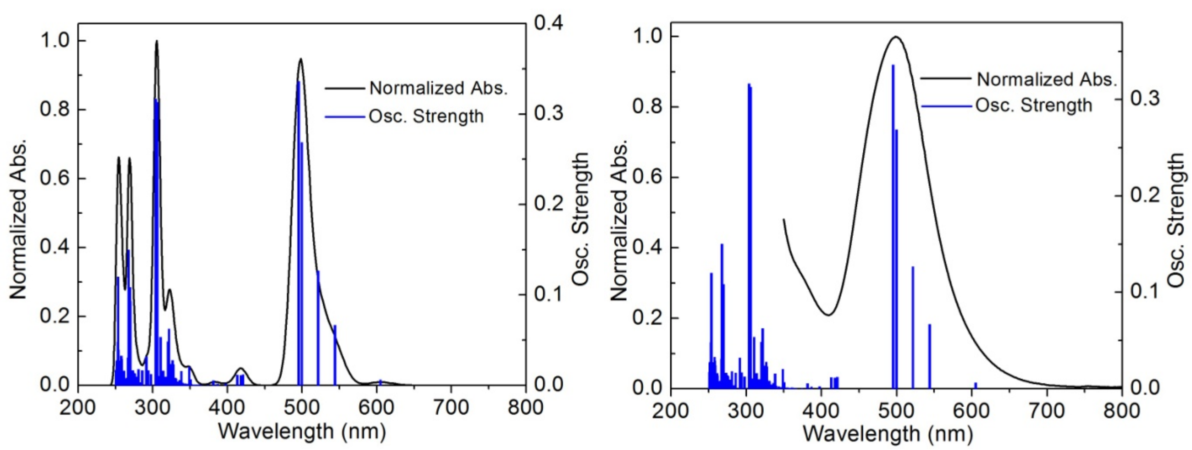

Figure S26. Left: Computed positions and oscillator strength for the 100st electronic transitions for **[Pd_3^{2+}]** (MeOH solvent field applied). The black line is generated by applying a thickness of 500 cm^{-1}. Right: Experimental UV-vis spectrum (in MeOH) and oscillator strength for the 100st electronic transitions for **[Pd_3^{2+}]** (MeOH solvent field applied).

DFT calculation results for **[Pd_3^{2+}]•••MCP** assembly

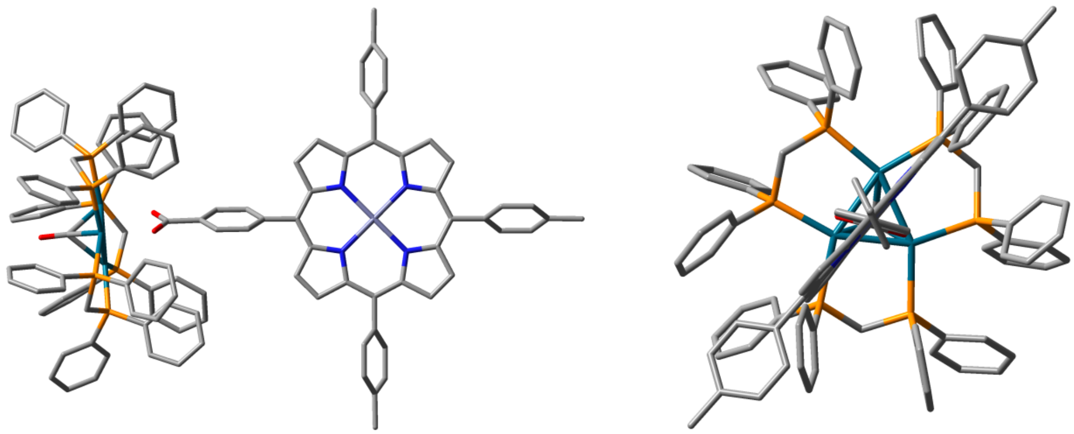

Side View Top View

Figure S27. Optimized geometry of **[Pd_3^{2+}]•••MCP** in MeOH solvent field. The computed Pd-Pd distances are 2.655 Å, 2.640 Å, and 2.624 Å; Pd•••O distances: 3.368 Å (1st O), 3.298 Å (1st O), 2.416 Å (1st O), 3.516 Å (2nd O), 3.175 Å (2nd O), 2.411 Å (2nd O).

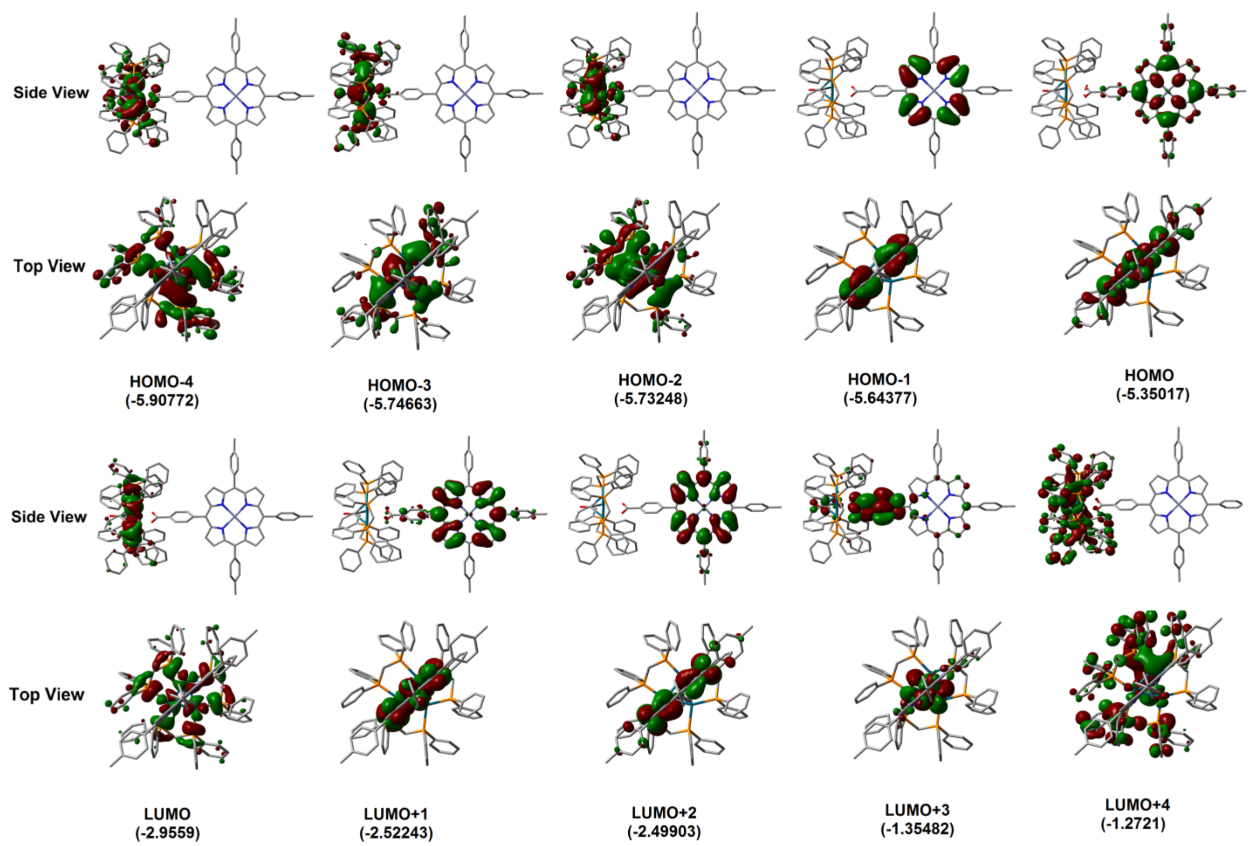

Figure S28. Representations of the frontier MOs of **[Pd_3^{2+}]•••MCP** in MeOH solvent field (energies in eV).

Table S5. Computed positions and oscillator strengths for the first 100 electronic transitions for **[Pd_3^{2+}]•••MCP** (MeOH solvent field applied).

No.	Wavelength (nm)	Osc. Strength	Major contributions (%)
1	682	0.0014	H-3→LUMO (57), H-2→LUMO (40)
2	616	0.0253	H-5→LUMO (38), H-3→LUMO (23), H-2→LUMO (35)
3	574	0.001	HOMO→LUMO (97)
4	541	0.0191	H-6→LUMO (71), H-4→LUMO (16)
5	527	0.0789	H-1→L+2 (33), HOMO→L+1 (67)
6	525	0.0397	H-1→L+1 (35), HOMO→L+2 (64)
7	519	0.2601	H-5→LUMO (28), H-4→LUMO (37), H-3→LUMO (10), H-2→LUMO (12)
8	505	0.0019	H-1→LUMO (98)
9	496	0.1747	H-8→LUMO (33), H-6→LUMO (15), H-5→LUMO (10), H-4→LUMO (31)
10	486	0.1743	H-8→LUMO (53), H-5→LUMO (13)
11	433	0.0017	H-17→LUMO (65), H-16→LUMO (14)
12	420	0.0009	H-2→L+1 (97)
13	417	0.015	H-3→L+1 (88)
14	417	0.0055	H-28→LUMO (31), H-27→LUMO (18), H-26→LUMO (18)
15	414	0.0004	H-2→L+2 (99)
16	411	0.0019	H-3→L+2 (98)
17	408	0.0574	H-32→LUMO (17), H-16→LUMO (15), H-15→LUMO (23)
18	405	0.0099	H-49→LUMO (11), H-20→LUMO (13), H-19→LUMO (11)
19	398	0.0306	H-50→LUMO (11), H-30→LUMO (10), H-18→LUMO (18)
20	397	0.4312	H-7→L+1 (40), H-4→L+1 (34), H-1→L+2 (16)
21	395	0.0453	H-7→L+1 (31), H-4→L+1 (63)
22	394	0.3823	H-7→L+2 (66), H-1→L+1 (21), HOMO→L+2 (10)
23	390	0.003	H-4→L+2 (98)
24	383	1.5805	H-7→L+1 (26), H-1→L+2 (43), HOMO→L+1 (22)
25	381	1.1194	H-7→L+2 (30), H-1→L+1 (41), HOMO→L+2 (24)
26	373	0.0243	H-30→LUMO (23), H-18→LUMO (26)
27	372	0.0001	H-7→LUMO (97)
28	370	0.0008	H-5→L+1 (98)
29	365	0.0001	H-5→L+2 (100)
30	353	0.0006	H-16→LUMO (20), H-15→LUMO (56)
31	350	0.0005	H-6→L+1 (98)
32	349	0	H-9→LUMO (95)
33	346	0.0004	H-12→LUMO (25), H-10→LUMO (48)
34	346	0.0003	H-13→L+1 (11), H-12→L+2 (12), H-9→L+1 (19), H-6→L+2 (44)
35	345	0.0092	HOMO→L+3 (58), HOMO→L+4 (10)
36	345	0.0016	H-9→L+1 (15), H-6→L+2 (56)
37	344	0.0009	H-10→LUMO (29)

38	343	0.0135	H-2→L+3 (27)
39	343	0.0014	H-13→LUMO (22), H-11→LUMO (52)
40	342	0.0006	H-12→LUMO (32)
41	341	0.0008	H-20→LUMO (14), H-19→LUMO (45), H-18→LUMO (19)
42	340	0.0013	H-19→LUMO (10), H-13→L+2 (10), H-12→L+1 (15), H-10→L+1 (12), H-9→L+2 (19)
43	340	0.0021	H-28→LUMO (10), H-20→LUMO (10), H-19→LUMO (12), H-9→L+2 (11)
44	337	0.0018	H-24→LUMO (23), H-22→LUMO (15), H-20→LUMO (29)
45	336	0.0044	H-32→LUMO (10), H-24→LUMO (37), H-22→LUMO (22)
46	335	0.0118	H-29→LUMO (12), H-14→LUMO (13), H-13→LUMO (21), H-11→LUMO (12)
47	335	0.0035	H-13→LUMO (46), H-11→LUMO (19)
48	335	0.0356	H-11→L+1 (86)
49	334	0.0649	H-10→L+1 (13), H-3→L+3 (19)
50	334	0.0205	H-11→L+2 (10), H-10→L+1 (40), H-9→L+2 (19)
51	333	0.031	H-26→LUMO (33), H-3→L+3 (11)
52	333	0.021	H-11→L+2 (47), H-8→L+1 (36)
53	332	0.0025	H-11→L+2 (24), H-10→L+1 (13), H-8→L+1 (50)
54	331	0.0002	H-14→LUMO (28)
55	331	0.0011	H-13→L+2 (21), H-12→L+1 (21), H-9→L+2 (35)
56	330	0.0022	H-31→LUMO (11), H-27→LUMO (32), H-10→L+2 (13)
57	330	0.0182	H-10→L+2 (57), H-9→L+1 (15)
58	329	0.0005	H-12→L+2 (39), H-9→L+1 (32), H-8→L+2 (15)
59	328	0.0001	H-8→L+2 (77)
60	327	0.0234	H-2→L+3 (19), H-2→L+4 (47)
61	325	0.0022	H-35→LUMO (15), H-32→LUMO (13), H-31→LUMO (20)
62	325	0	H-13→L+1 (61), H-12→L+2 (25)
63	324	0.0369	H-3→L+4 (11), HOMO→L+4 (17)
64	323	0.0047	HOMO→L+3 (11), HOMO→L+4 (60)
65	322	0.0344	H-3→L+4 (14), H-2→L+5 (12)
66	321	0.0163	H-37→LUMO (10), H-34→LUMO (35), H-30→LUMO (17)
67	320	0.0091	H-36→LUMO (44), H-34→LUMO (12)
68	320	0.0874	H-3→L+4 (17)
69	319	0.0221	H-13→L+2 (46), H-12→L+1 (38)
70	319	0.0358	H-1→L+3 (77), H-1→L+4 (14)
71	318	0.0126	H-4→L+3 (14), H-4→L+4 (11), H-3→L+3 (15), H-3→L+5 (15)
72	317	0.0577	H-14→L+1 (72)
73	316	0.0068	H-37→LUMO (29), H-36→LUMO (16)
74	316	0.0067	H-14→L+2 (71)
75	316	0.0384	H-38→LUMO (16)
76	316	0.0266	H-40→LUMO (15), H-2→L+5 (12)
77	315	0.0011	H-44→LUMO (11), H-39→LUMO (23), H-38→LUMO (15), H-34→LUMO (11)

78	314	0.0218	H-39→LUMO (22), H-38→LUMO (26)
79	314	0.0082	H-40→LUMO (19), H-39→LUMO (17)
80	313	0.0059	HOMO→L+5 (71), HOMO→L+6 (16)
81	313	0.0001	H-22→LUMO (14), H-21→LUMO (54)
82	312	0.001	H-41→LUMO (75)
83	311	0.0603	HOMO→L+5 (12), HOMO→L+6 (34)
84	311	0.0262	H-25→LUMO (12), HOMO→L+6 (19)
85	311	0.0067	H-25→LUMO (83)
86	310	0.0503	H-2→L+6 (21)
87	310	0.0184	H-42→LUMO (29)
88	309	0.031	H-43→LUMO (13)
89	309	0.0109	HOMO→L+9 (55)
90	309	0.0011	H-23→LUMO (30)
91	308	0.0009	H-23→LUMO (61)
92	308	0.0103	H-44→LUMO (15), H-43→LUMO (11), H-42→LUMO (21), H-2→L+6 (13)
93	307	0.0154	H-3→L+5 (12), H-3→L+6 (32)
94	306	0.0127	H-48→LUMO (10)
95	305	0.0032	HOMO→L+7 (75)
96	304	0.006	H-33→LUMO (50), H-31→LUMO (10)
97	304	0.0011	H-47→LUMO (12), H-45→LUMO (16), H-2→L+7 (13)
98	303	0.0469	H-4→L+4 (11), H-4→L+5 (12)
99	303	0.0098	H-46→LUMO (16), H-45→LUMO (10), H-3→L+8 (11), HOMO→L+8 (10)
100	303	0.0009	H-23→L+1 (77), H-21→L+2 (11)

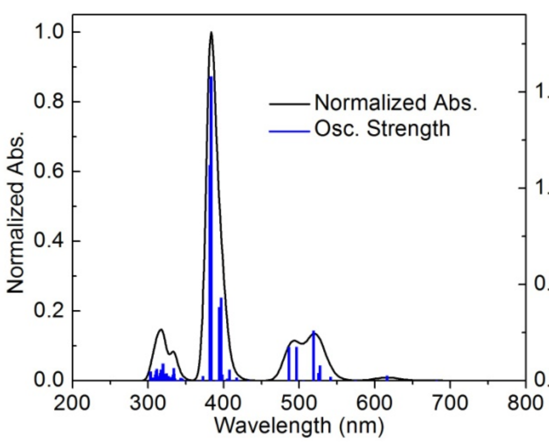

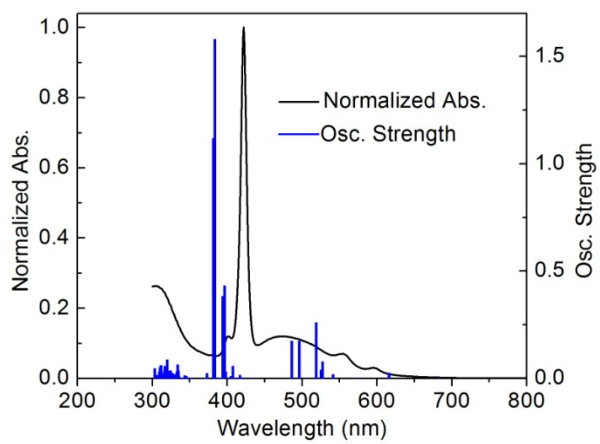

Figure S29. Left: Computed positions and oscillator strength for the 100st electronic transitions for **[Pd_3^{2+}] •••MCP** (MeOH solvent field applied). The black line is generated by applying a thickness of 500 cm^{-1}. Right: Experimental UV-vis spectrum and oscillator strength for the 100st electronic transitions for **[Pd_3^{2+}] •••MCP** (MeOH solvent field applied). The experimental UV-vis spectrum was recorded under 1 eq. **[MCP]** *vs* 8 eq. **[Pd_3^{2+}]** in MeOH.

DFT calculation results for **[Pd_3^{2+}]•••DCP•••[Pd_3^{2+}]** assembly

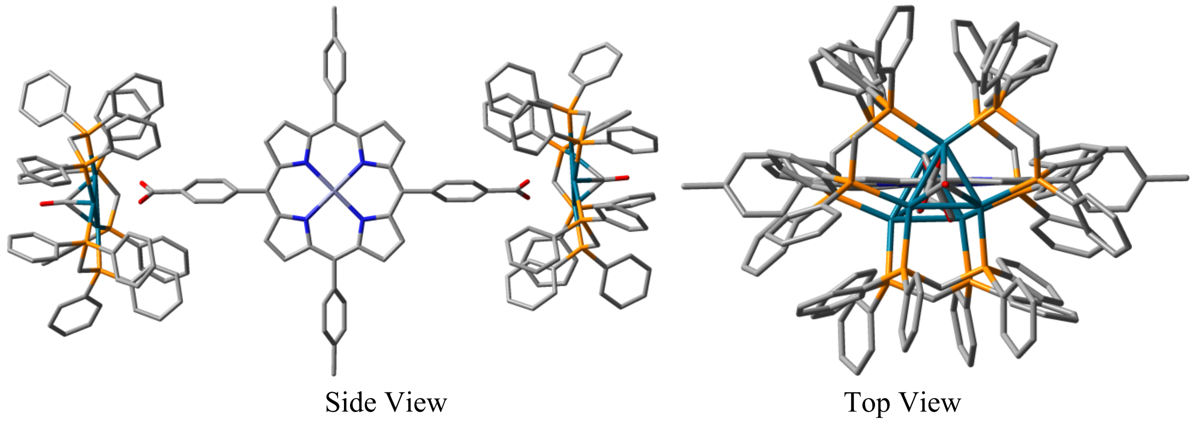

Figure S30. Optimized geometry of **[Pd_3^{2+}]•••DCP•••[Pd_3^{2+}]** in MeOH solvent field. The computed Pd-Pd distances are 2.658 Å, 2.642 Å, and 2.624 Å in the left; 2.659 Å, 2.641 Å, and 2.624 Å in the right; Pd•••O distances in left hand: 3.365 Å (1st O), 3.318 Å (1st O), 2.411 Å (1st O), 3.518 Å (2nd O), 3.179 Å (2nd O), 2.417 Å (2nd O); Pd•••O distances in right hand: 3.366 Å (1st O), 3.320 Å (1st O), 2.411 Å (1st O), 3.518 Å (2nd O), 3.179 Å (2nd O), 2.417 Å (2nd O). The introduction of second palladium cluster has almost no effect on the porphyrin-cluster assembly.

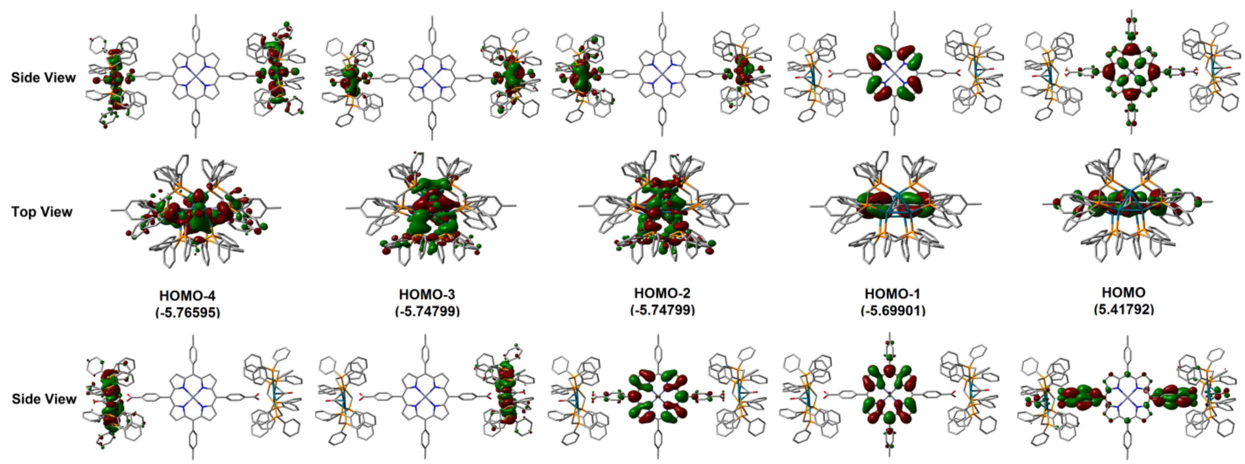

Figure S31. Representations of the frontier MOs of **[Pd_3^{2+}]•••DCP•••[Pd_3^{2+}]** in MeOH solvent field (energies in eV).

Table S12. Computed positions and oscillator strengths for the first 100 electronic transitions for **[Pd_3^{2+}]•••DCP•••[Pd_3^{2+}]** (MeOH solvent field applied).

No.	Wavelength (nm)	Osc. Strength	Major contributions (%)
1	668	0.0014	H-4->L+1 (45), H-2->L+1 (49)
2	668	0.0014	H-5->LUMO (45), H-3->LUMO (49)
3	629	0.0015	HOMO->LUMO (96)
4	629	0.0015	HOMO->L+1 (95)
5	607	0.0036	H-9->LUMO (10), H-8->L+1 (25), H-4->L+1 (23), H-2->L+1 (18)
6	607	0.0302	H-9->LUMO (25), H-8->L+1 (10), H-5->LUMO (23), H-3->LUMO (18)
7	566	0	H-1->LUMO (100)
8	565	0	H-1->L+1 (100)
9	532	0.0035	H-12->LUMO (17), H-11->L+1 (52), H-6->L+1 (13)
10	532	0.037	H-12->LUMO (52), H-11->L+1 (17), H-7->LUMO (13)
11	524	0.0813	H-1->L+3 (34), HOMO->L+2 (65)
12	519	0.0121	H-1->L+2 (42), HOMO->L+3 (57)
13	513	0.142	H-8->L+1 (12), H-7->LUMO (13), H-6->L+1 (38)
14	513	0.2816	H-9->LUMO (12), H-7->LUMO (37), H-6->L+1 (12)
15	492	0.0879	H-15->LUMO (50), H-9->LUMO (17), H-7->LUMO (13)
16	492	0.0898	H-14->L+1 (50), H-8->L+1 (17), H-6->L+1 (13)
17	477	0.0909	H-15->LUMO (20), H-14->L+1 (18), H-9->LUMO (12), H-8->L+1 (10)
18	477	0.2684	H-15->LUMO (18), H-14->L+1 (20), H-9->LUMO (11), H-8->L+1 (12)
19	465	0	H-2->LUMO (100)
20	464	0	H-3->L+1 (100)
21	457	0	H-4->LUMO (96)
22	456	0	H-5->L+1 (96)
23	440	0	H-6->LUMO (96)
24	440	0	H-7->L+1 (96)
25	424	0.0021	H-43->LUMO (17), H-41->LUMO (11), H-34->LUMO (13), H-29->LUMO (18)
26	424	0.002	H-43->L+1 (15), H-41->L+1 (12), H-34->L+1 (12), H-29->L+1 (20)
27	411	0.0025	H-51->LUMO (12), H-47->LUMO (20), H-46->LUMO (16)
28	411	0.0024	H-50->L+1 (10), H-47->L+1 (19), H-46->L+1 (21)
29	403	0.0284	H-25->LUMO (11)
30	402	0.0523	H-24->L+1 (10)
31	401	0	H-8->LUMO (100)
32	400	0	H-9->L+1 (100)
33	400	0.0013	
34	400	0.0145	
35	393	0.0725	
36	393	0.0175	
37	392	0.0096	H-10->LUMO (86)
38	392	0.0065	H-10->L+1 (88)

39	392	0.0014	H-2->L+2 (92)
40	391	0.0033	H-3->L+2 (94)
41	391	0.4483	H-10->L+2 (61), H-1->L+3 (15)
42	386	0.1196	H-5->L+2 (36), H-4->L+2 (50)
43	385	0.0117	H-5->L+2 (53), H-4->L+2 (45)
44	384	0.2439	H-10->L+3 (67), H-1->L+2 (17), HOMO->L+3 (10)
45	380	0.0199	H-2->L+3 (98)
46	379	0.0357	H-3->L+3 (97)
47	379	1.371	H-10->L+2 (18), H-1->L+3 (28), HOMO->L+2 (16)
48	378	0	H-11->LUMO (94)
49	377	0	H-12->L+1 (93)
50	374	0.0285	H-13->LUMO (50), H-5->L+3 (13), H-4->L+3 (26)
51	374	0.0385	H-13->LUMO (42), H-5->L+3 (17), H-4->L+3 (31)
52	374	0.0002	H-13->L+1 (91)
53	374	0.0107	H-5->L+3 (59), H-4->L+3 (38)
54	373	0.0044	H-7->L+2 (16), H-6->L+2 (83)
55	373	0.0091	
56	373	0.0127	
57	372	0.099	H-7->L+2 (67), H-6->L+2 (13)
58	371	0.6769	H-10->L+3 (23), H-1->L+2 (31), HOMO->L+3 (22)
59	367	0.0009	H-19->L+1 (17), H-16->L+1 (69)
60	367	0.0004	H-19->LUMO (19), H-16->LUMO (67)
61	365	0.0001	H-18->LUMO (21), H-17->LUMO (71)
62	365	0.0001	H-17->L+1 (91)
63	363	0.0001	HOMO->L+4 (84), HOMO->L+6 (10)
64	363	0.0021	H-6->L+3 (93)
65	363	0.0124	H-7->L+3 (95)
66	362	0.0002	H-18->LUMO (61), H-17->LUMO (17), H-14->LUMO (17)
67	361	0.0002	H-18->L+1 (76), H-15->L+1 (18)
68	359	0.0011	H-22->LUMO (41), H-21->LUMO (19)
69	359	0.0012	H-22->L+1 (12), H-21->L+1 (47)
70	358	0	H-19->LUMO (49), H-16->LUMO (12), H-14->LUMO (29)
71	358	0	H-19->L+1 (51), H-16->L+1 (10), H-15->L+1 (29)
72	357	0	H-19->LUMO (28), H-16->LUMO (11), H-14->LUMO (49)
73	357	0	H-19->L+1 (28), H-18->L+1 (10), H-16->L+1 (10), H-15->L+1 (49)
74	350	0.2399	H-1->L+3 (10), HOMO->L+5 (49), HOMO->L+7 (17)
75	350	0.0072	H-27->LUMO (21), H-25->LUMO (15)
76	350	0.0125	H-26->L+1 (20), H-24->L+1 (14)
77	347	0.0001	H-33->LUMO (22), H-27->LUMO (31), H-25->LUMO (14)
78	347	0.0002	H-31->L+1 (21), H-26->L+1 (28), H-24->L+1 (15)
79	347	0.0021	H-32->LUMO (37)
80	347	0.0015	H-30->L+1 (40), H-26->L+1 (12)
81	346	0.0013	H-8->L+2 (78)

82	346	0.0039	H-9->L+2 (79)
83	346	0	H-19->L+2 (28), H-17->L+3 (23), H-13->L+2 (44)
84	344	0.0004	H-39->L+1 (13), H-31->L+1 (40)
85	344	0.0004	H-39->LUMO (15), H-33->LUMO (12), H-32->LUMO (27)
86	342	0.0103	H-2->L+4 (17), H-2->L+5 (25)
87	342	0.0058	H-3->L+4 (19), H-3->L+5 (24)
88	342	0.0006	H-35->L+1 (58)
89	342	0.0006	H-36->LUMO (57)
90	341	0	H-1->L+4 (86), H-1->L+6 (11)
91	341	0.0015	H-44->L+1 (10), H-43->L+1 (13), H-35->L+1 (15), H-20->L+1 (13)
92	340	0.0014	H-43->LUMO (13), H-36->LUMO (14), H-20->LUMO (13)
93	340	0.0001	H-19->L+3 (17), H-17->L+2 (53), H-13->L+3 (23)
94	339	0.0002	H-40->L+1 (13), H-37->L+1 (28), H-20->L+1 (11)
95	339	0.0002	H-41->LUMO (10), H-38->LUMO (18), H-37->LUMO (15), H-20->LUMO (12)
96	337	0.0021	H-42->LUMO (45), H-40->L+1 (11), HOMO->L+6 (10)
97	337	0.0003	H-42->LUMO (15), H-40->L+1 (41)
98	337	0.0005	HOMO->L+6 (73)
99	336	0.0422	H-16->L+2 (88)
100	336	0.0002	H-8->L+3 (11), HOMO->L+5 (26), HOMO->L+7 (53)

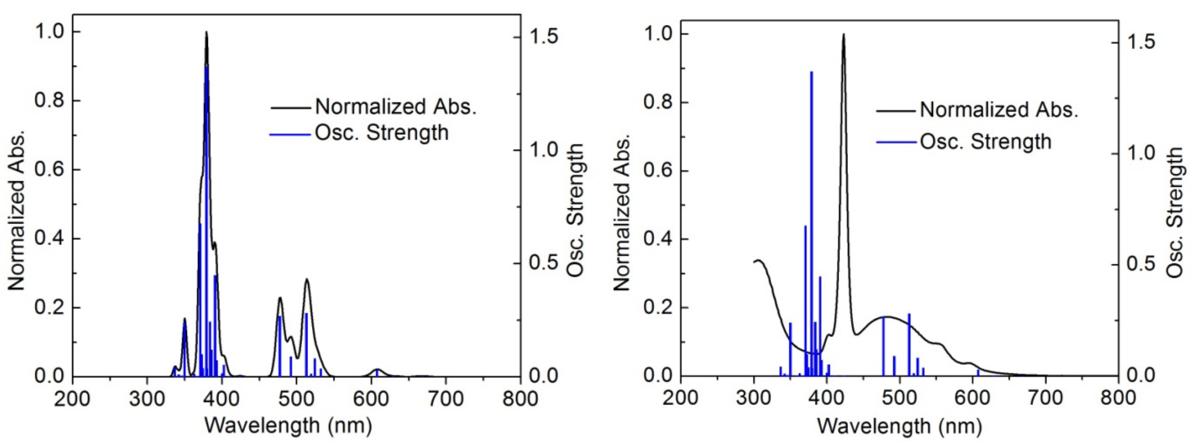

Figure S32. Left: Computed positions and oscillator strength for the 100st electronic transitions for **[Pd_3^{2+}]•••DCP•••[Pd_3^{2+}]** (MeOH solvent field applied). The black line is generated by applying a thickness of 500 cm^{-1}. Right: Experimental UV-vis spectrum and oscillator strength for the 100st electronic transitions for **[Pd_3^{2+}]•••DCP•••[Pd_3^{2+}]** (MeOH solvent field applied). The experimental UV-vis spectrum was recorded under 1 eq. **[DCP]** *vs* 4 eq. **[Pd_3^{2+}]** in MeOH.

Fs transient absorption spectroscopy

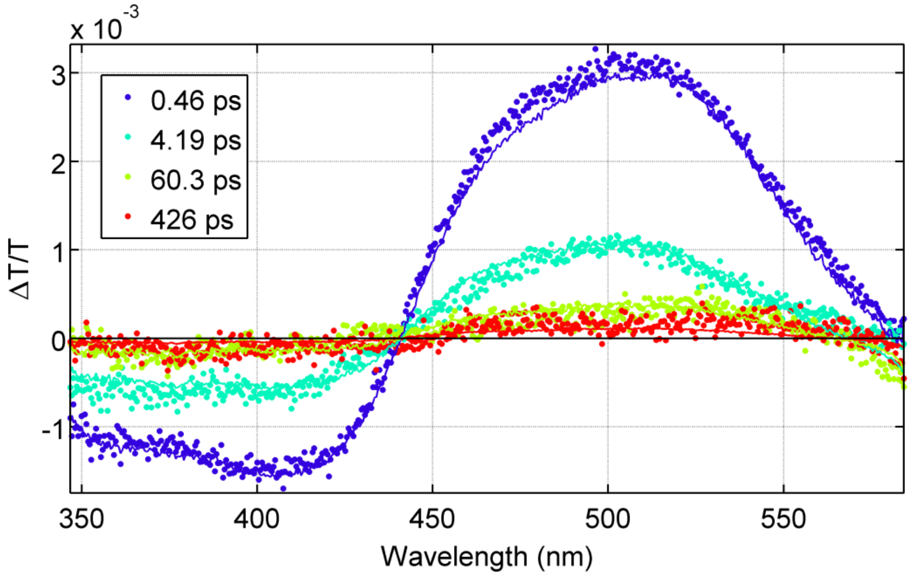

Figure S33. TAS spectra of **[Pd_3^{2+}]** in MeOH at 298 K as a function of delay time between the pump and probe laser pulses.

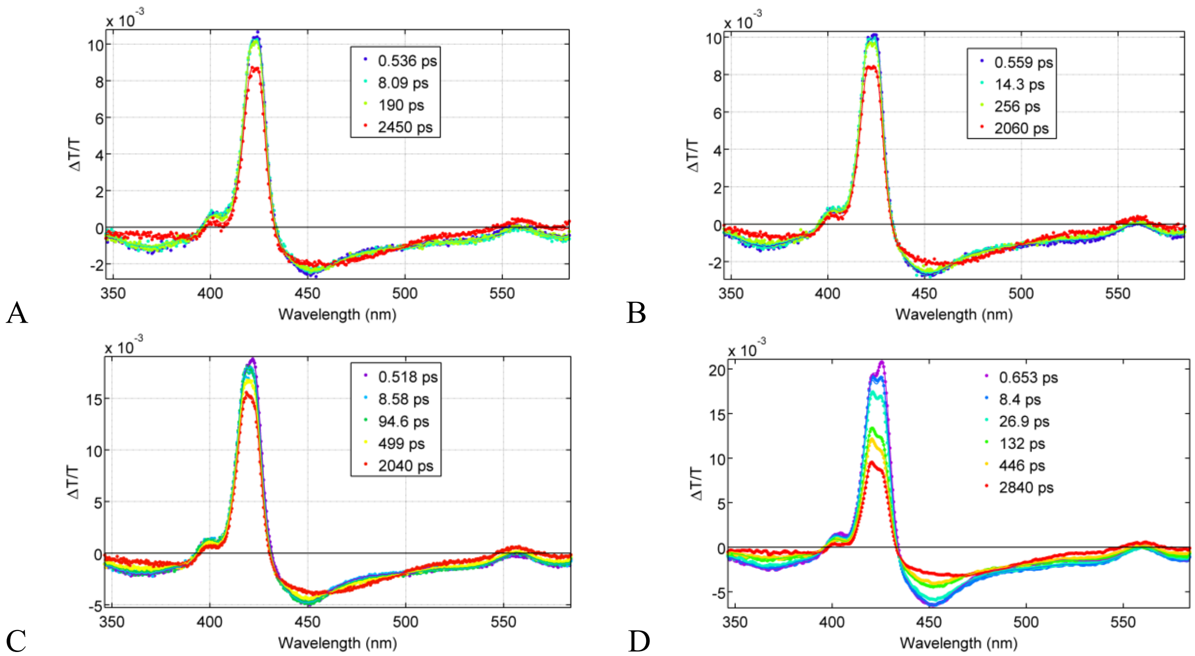

Figure S34. TAS of **MCP** (A), and **MCP** with 1 (B), 2 (C), and 4 (D) eqs. of **[Pd_3^{2+}]** in MeOH at 298 K as a function of delay time between the pump and probe laser pulses.

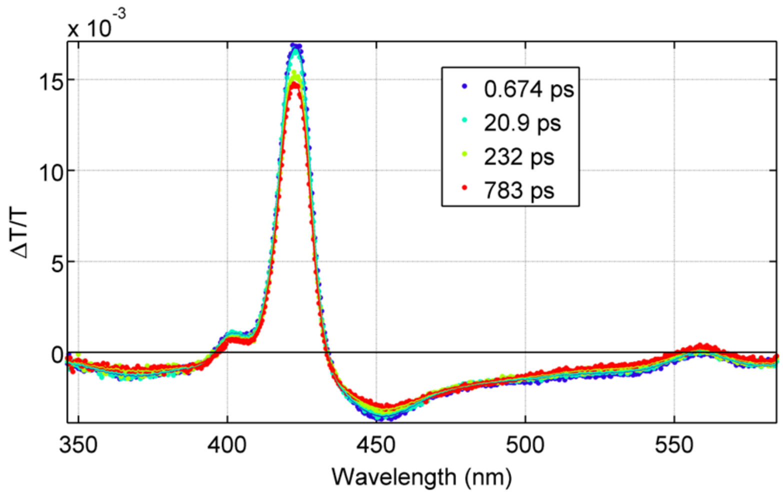

A

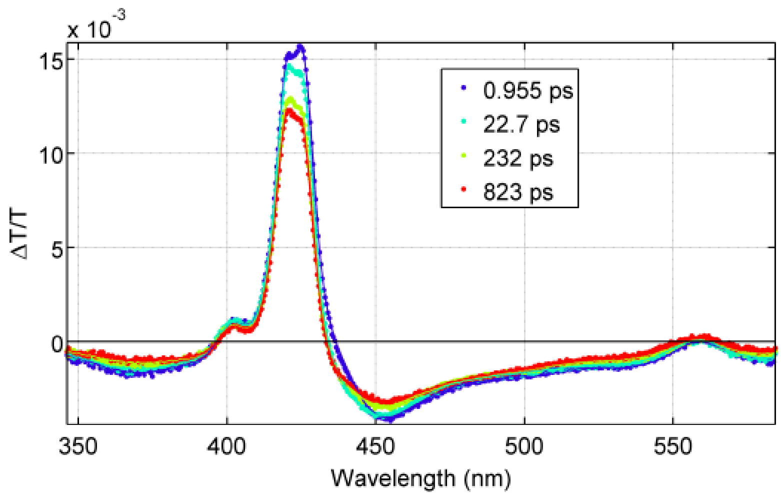

B

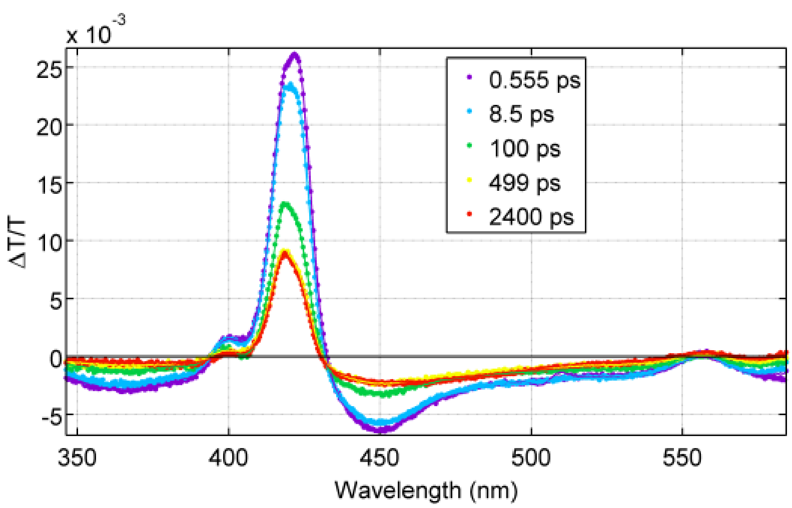

C

Figure S35. TAS of **DCP** (A), and **DCP** with 1 (B) and 2 (C) eqs. of **[Pd_3^{2+}]** in MeOH at 298 K as a function of delay time between the pump and probe laser pulses.

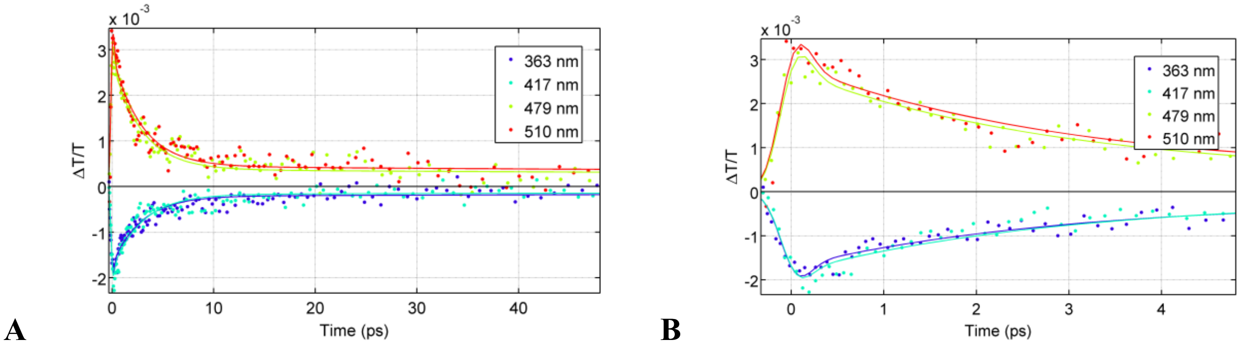

Figure S36. Decay traces of the TAS signal monitored at different wavelengths for **[Pd_3^{2+}]** in MeOH at 298 K as a function of delay time between the pump and probe laser pulses.

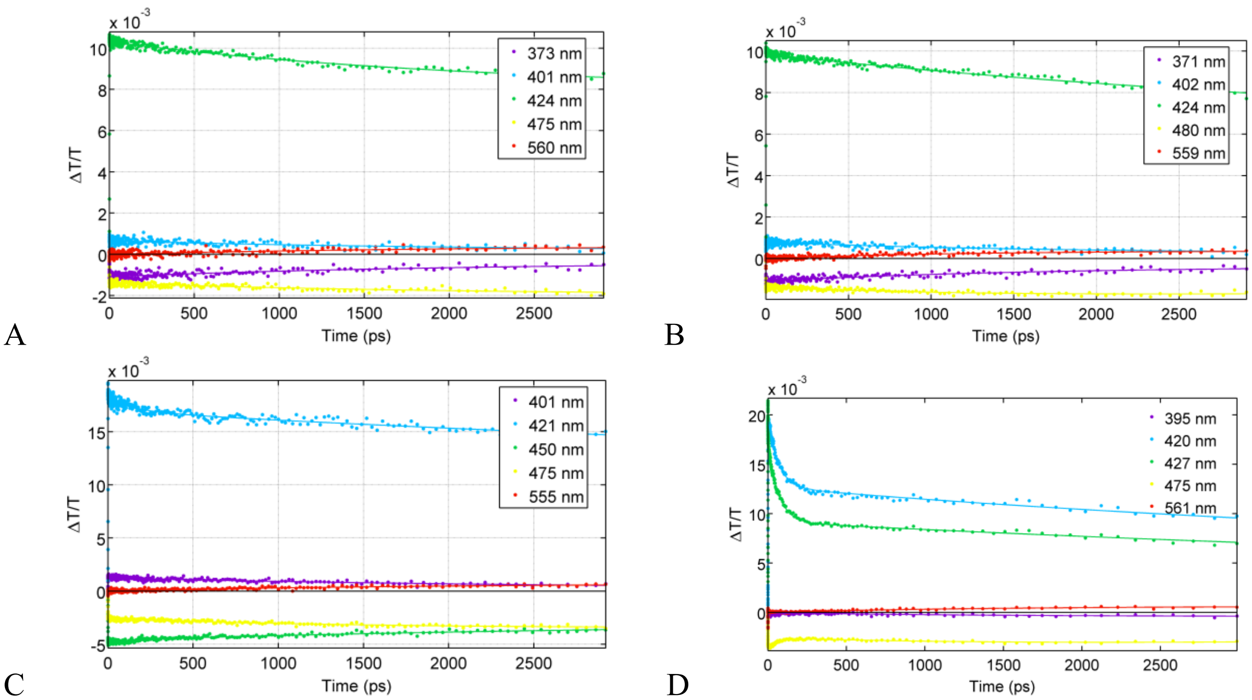

Figure S37. Decay traces of the TAS signal monitored at different wavelengths for **MCP** (A), and **MCP** with 1 (B), 2 (C), and 4 (D) eqs. of **[Pd_3^{2+}]** in MeOH at 298 K as a function of delay time between the pump and probe laser pulses.

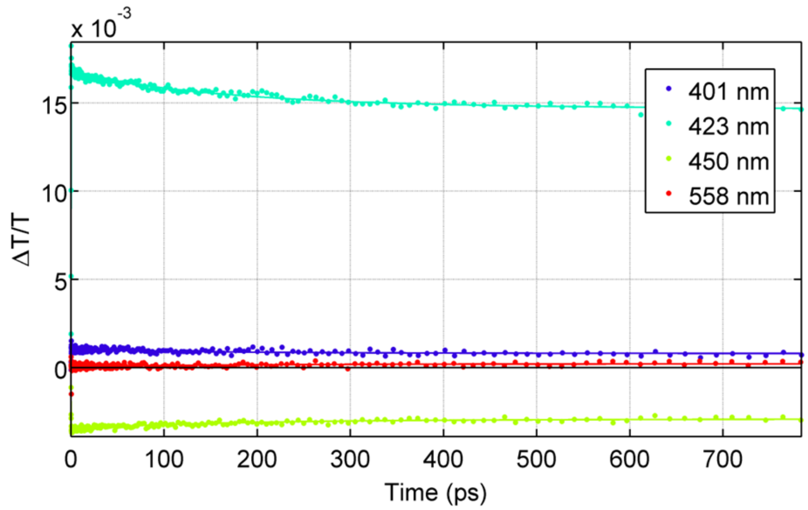

A

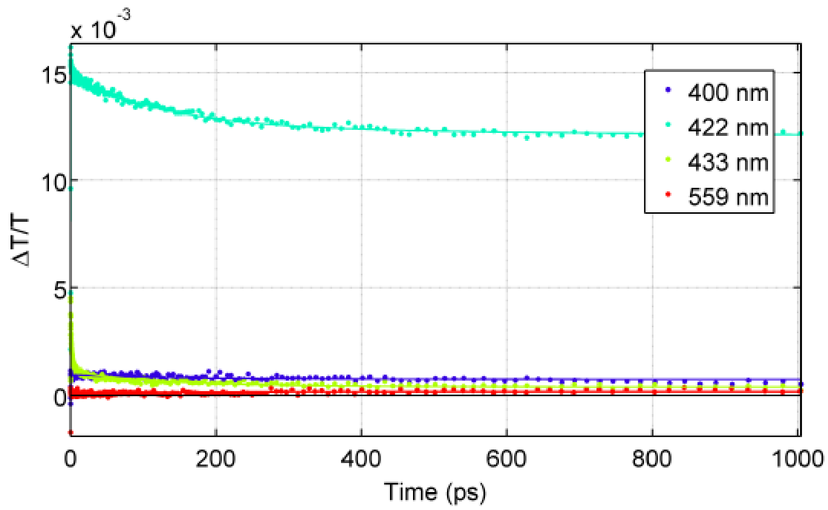

B

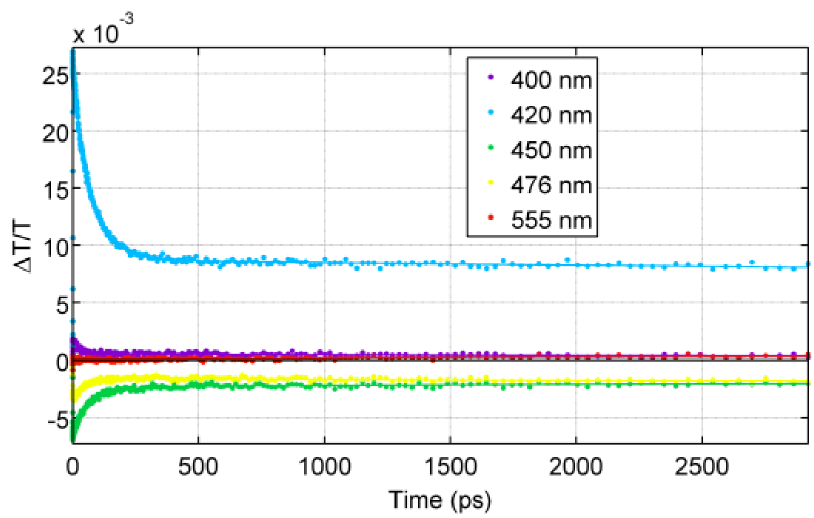

C

Figure S38. Decay traces of the TAS signal monitored at different wavelengths for **DCP** (A), and **DCP** with 1 (B) and 2 (C) eqs. of **[Pd_3^{2+}]** in MeOH at 298 K as a function of delay time between the pump and probe laser pulses.